RÔMULO LUZ CORTEZ

Topology Optimization of Structures Considering Soil-Structure Interaction

São Paulo
2022

RÔMULO LUZ CORTEZ

Topology Optimization of Structures Considering Soil-Structure Interaction

Revised Version

Dissertation presented to the Polytechnic School of the University of São Paulo to obtain the title of Master of Science in Mechanical Engineering.

Field of Study:

Mechanical Engineering of Design and Manufacturing (3151)

Supervised by:

Prof. Dr. Renato Picelli Sanches

São Paulo
2022

Este exemplar foi revisado e corrigido em relação à versão original, sob responsabilidade única do autor e com a anuência de seu orientador.

São Paulo, 26 de agosto de 2022

Assinatura do autor: Rômulo Luz Cortez

Assinatura do orientador: Renato Pavanello Sanches

Catalogação-na-publicação

Cortez, Rômulo Luz
Topology Optimization of Structures Considering Soil-Structure Interaction / R. L. Cortez -- versão corr. -- São Paulo, 2022.
77 p.

Dissertação (Mestrado) - Escola Politécnica da Universidade de São Paulo. Departamento de Engenharia Mecânica.

1.Topology Optimization 2.Soil-Structure Interaction 3.TOBS method 4.Finite Element Method 5.Boundary Element Method I.Universidade de São Paulo. Escola Politécnica. Departamento de Engenharia Mecânica II.t.

ACKNOWLEDGMENTS

Agradeço ao meu orientador Prof. Dr. Renato Picelli Sanches pela sua competente orientação, pela paciência, pelo exemplo de profissional e ser humano, pela determinação e pela amizade.

Aos meus pais Antonio Francisco Gomes Cortez e Rosemeire Luz Cortez por tudo, e ao meu Irmão, Rafael Luz Cortez, que juntos, são minha base. Eu teria que ter muitas páginas para agradecê-los devidamente.

Ao meu amor, Larissa Thaís de Araújo Machado, pelo apoio incondicional nas noites em claro, pela paciência, pela integral assistência e companheirismo nas melhores e piores horas.

Ao meu amigo Lucas Oliveira Siqueira por ser um incentivador e também um exemplo de motivação e humildade.

Ao Prof. Dr. Josué Labaki da Faculdade de Engenharia Mecânica da UNICAMP, pelo apoio acadêmico.

Aos meus colegas de grupo de pesquisa por estarem sempre dispostos a ajudar.

À Prof. Dr. Simone dos Santos Hoefel da Universidade Federal do Piauí, pela indicação à bolsa e pelo exemplo de profissionalismo e dedicação.

À Escola Politécnica da Universidade de São Paulo pela oportunidade de realização do curso de mestrado.

À Fundação de Amparo à Pesquisa do Estado de São Paulo por propiciar as condições financeiras de realizar a pesquisa.

E a todos os que de forma direta e indireta ajudaram na conclusão desta dissertação.

RESUMO

A otimização topológica abre novas perspectivas para o projeto de engenharia estrutural por meio de layouts otimizados. A ideia é encontrar layouts estruturais com desempenho aprimorado independente da experiencia do projetista. Conforme a complexidade das condições de contorno aumenta, novos métodos computacionais precisam ser desenvolvidos. Uma classe de problemas inexplorados diz respeito ao projeto de estruturas sobre solo elástico em contrapartida a suportes rígidos. Neste contexto, este projeto de mestrado propõe e investiga o método de otimização topológica aplicado a problemas de interação solo-estrutura. Neste esquema, o solo e a estrutura são modelados separadamente com o Método dos Elementos de Contorno Indiretos (IBEM do inglês *Indirect Boundary Element Method*) e com o Método dos Elementos Finitos (FEM do inglês *Finite Element Method*), respectivamente. A resposta da estrutura interagindo com o solo é obtida impondo condições de continuidade e equilíbrio na interface. O método de Otimização Topológica de Estruturas Binárias (TOBS do inglês *Topology Optimization of Binary Structures*) é escolhido para resolver o problema de maximização da rigidez de uma estrutura sujeita a uma restrição de volume. Os resultados numéricos mostram que os efeitos da iteração solo-estrutura são relevantes ao projetar uma estrutura via otimização topológica para diferentes razões de rigidez estrutura-solo. Além disso, os resultados mostram que a presença de vazios no solo altera sua flexibilidade, independentemente das propriedades constitutivas do solo e que isso altera significativamente a estrutura otimizada.

Palavras-Chave – Otimização Topológica, Interação Solo-estrutura, TOBS, Método dos Elementos Finitos, Método dos Elementos de Contorno.

ABSTRACT

Topology optimization opens up new perspectives for structural engineering design via optimized layouts. The idea is to find structural layouts with improved performance regardless of the designer's experience. As the complexity of boundary conditions increase, new computational methods are required to be developed. One class of unexplored problems concerns the design of structures resting on elastic soil instead of rigid supports. In that context, this master by research project proposes and investigates the topology optimization method applied to soil-structure interaction problems. In this scheme, the soil and the structure are modeled separately with the Indirect Boundary Element Method (IBEM) and with the Finite Element Method (FEM), respectively. The response of the structure interacting with the soil is obtained by imposing continuity and equilibrium conditions at their interface. The Topology Optimization of Binary Structures (TOBS) method is chosen to solve the structural stiffness maximization problem subject to a volume constraint. Numerical results show that the effects of the soil-structure iteration are relevant when designing a structure via topological optimization for different structure-soil stiffness ratios. Furthermore, the results show that the presence of voids in the soil alters its flexibility, regardless of the constitutive properties of the soil and that this significantly alters the optimized structure.

Keywords – Topology Optimization, Soil-Structure Interaction, TOBS, Finite Element Method, Boundary Element Method.

LIST OF FIGURES

LIST OF TABLES

CONTENTS

1 INTRODUCTION

1.1 Soil-Structure Interaction

Static response of a structure can be significantly changed depending on the soil profile where it is fixed. The consideration of soil elasticity is generally not taken into account in the optimization design of structures. However, for macro structures, for structures sensitive to small displacements and vibrations, or when the structure is installed in softer marine soil, for example, inclusion of this consideration becomes more important. On the other hand, the soil influence in the structural Topology Optimization (TO) is often neglected. Major uncertainties about its conditions justify why this parameter has not been sufficiently addressed in design optimization. Therefore, Soil-Structure Interaction (SSI) defines a relevant phenomenon for structural design and must be taken into account on TO problems.

Given the current interest of this topic, the literature is scarce regarding the influence of the soil in the TO. Figures 1 and 2 show selected examples of soil-structure interaction problems, which illustrate the need of considering the influence of soil flexibility in the structural analysis. These examples consider a structure under uniformly distributed horizontal and vertical loads, supported by a rigid base and resting on the surface of the elastic soil. The color map shows the normal strain in the vertical direction. The comparison of these results shows that the displacement and strain field of the structure are strongly affected by the presence of soil. This suggests that optimal topologies for the structure will depend on whether or not the presence of the soil is taken into consideration in the analysis.

Figure 1: Displacement and strain fields of a structure under uniformly distributed horizontal load supported by:

(a) a rigid base. (b) the elastic soil.

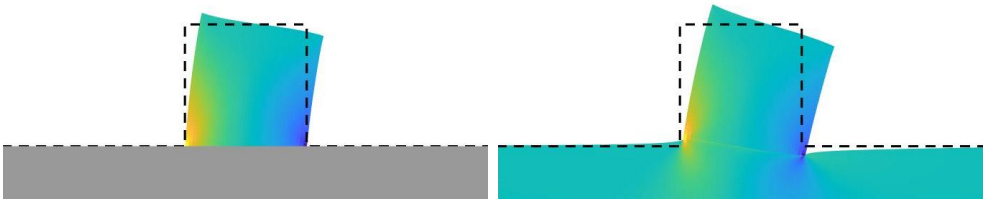

Figure 2: Displacement and strain fields of a structure under uniformly distributed vertical load supported by:

(a) a rigid base. (b) the elastic soil.

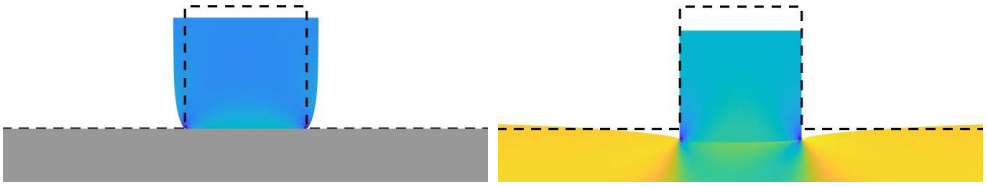

The aim of this dissertation is to investigate how the flexibility of the soil affects the TO of the structure in a static SSI problem. This is an important consideration when designing a structure via TO in problems in which the influence of the soil is significant, such as particle accelerators buildings, nuclear power plants, and offshore structures on seabed.

In this work, the soil is modeled as a homogeneous, isotropic, elastic half-space, on the surface of which rests an arbitrarily-shaped structure. The static response of the soil is obtained by superposition of Green's functions for the unbounded medium, in the sense of the Indirect Boundary Element Method (IBEM). This enables accurate representation of the load transfer between soil and structure through their continuous contact interface. Differently than a Finite Element Method (FEM) discretization, for the soil part, this IBEM scheme requires only the one-dimensional contact interface to be discretized. Coupling between the FEM model of the structure and the IBEM model of the soil is obtained by imposing rigorous equilibrium and continuity conditions at the interface.

1.2 Justification

The influence of soil displacement is important in the design of structures that are sensitive even to micro-displacements from soil such as nuclear power plants, particle accelerators, gravitational waves observatory, etc., and where the soil elasticity must be take into consideration, such as offshore platforms and offshore wind turbines. Literature is scarce on TO considering the elasticity of the soil. Most works consider the soil as a rigid boundary condition or an elastic spring representing the behavior of the soil. In other works, more sophisticated FEM models were developed [1].

The IBEM allows the discretization of infinite domains with a finite number of elements located in the soil-structure interface. The response at any point in that domain is

exact and the method is more formal than the FEM. Furthermore, in dynamic problems, the FEM presents the problem of reflection on the edge of discretization, bringing errors, or leading to the need for additional implementations to circumvent this problem. Considering the possibility of future works including dynamic analysis and the formalism of the method, the IBEM was chosen.

The main purpose of topology optimization is to find the ideal material distribution of a structure subject to known constraints, loads and final material volume within a specified design domain [2]. The optimization of structures subject to soil influence allows for material savings. This potential can be widely applied when of more complex manufacturing techniques are developed and applied largely in the market. Some works have been developed into civil construction field using 3D printing of cementitious composites [3]. They showed that 3D printing technology for cementitious materials is a promising alternative to revolutionize the conventional building and construction process through low-cost, high-efficient automatic construction and design freedom given by optimization algorithms.

In the future, optimized layouts that bring weight and structural performance optimizations will be a priority for designers and will bring savings in project costs. Currently, the fabrication costs of structures with complex geometries are still not always enough to justify the choice of an optimized design. However, in the future, technologies such as additive manufacturing and 3D printing will become increasingly accessible. Topology optimization will provide the best designs for fabrication of structures to be built through these processes.

Many optimization methods have been developed within the last decades. Binary topology optimization methods defines the structure using a pixel-like definition. A useful design variable called pseudo-density (ρ) is stated as 1 if the element is solid or 0 when the element is void. Topology Optimization of Binary Structures (TOBS) method, developed by Sivapuram and Picelli [4] was used. The advantages of TOBS are the clear definition of the boundary and the possibility to deal with multiphysics, multiobjective and multimaterial optimization.

1.3 Objectives

Based on the discussed academic scenario, the **aim** of this dissertation is to solve topology optimization problems considering soil-structure interaction. Instead of classical

density-based methods, the TOBS method will be adopted, owing to the potential performance improvement of binary design variables. In addition, IBEM is used to model soil behavior.

The **objectives** are:

1. To couple soil and structure models;
2. To perform topology optimization using the TOBS method for different structure-to-soil flexibility ratios;
3. To understand the influence of soil flexibility in optimum structural design.

1.4 Layout of the Work

This document is organized as follows. Chapter 2 presents the literature review with analysis of the relevant literature already published in the areas of soil modeling, and topology optimization. Chapter 3 presents the problem governing equations, the algebraic system used in the finite element method and the boundary element method, the optimization parameters and definitions, and the TOBS method. Chapter 4 presents the structural problem to be solved, the soil-structure coupling, and the optimization sensitivity analysis is performed. In Chapter 5, numerical results obtained are presented, comparing different structure-to-soil elasticity relations and parameters. Finally, chapter 6, presents the main conclusions of this research, suggested future works, and discussions.

2 LITERATURE REVIEW

This chapter presents the literature review with analysis of the relevant literature of soil modeling, and topology optimization. It serves as a basis for the investigation of the proposed work.

2.1 Soil Modeling

In practice, soil is a heterogeneous, non-linear and anisotropic medium. Also, the presence of fluctuation of water table further adds to its complexity. Therefore, it would be very complex and costly to model soil medium taking into account all these characteristics [5]. Soil can be modeled in a number of ways with various levels of rigor. In this context, the simplicity of models often becomes a primary consideration and often yields reasonable results [6].

The first idealization of a linear-elastic soil model was proposed by Winkler [7]. Winkler models the soil as a system of identical but mutually independent, closely spaced, discrete, linearly elastic springs. Figure 3 shows the physical representation of the Winkler foundation.

Figure 3: The Winkler foundation.

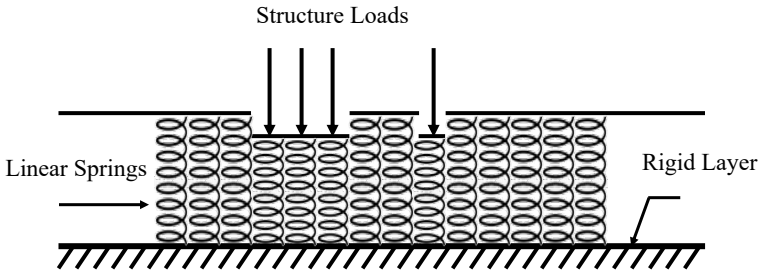

Diagram by Author.

In this model, as we can see in the figure 3, the soil is deformed only in the region where there is loading. Neighboring regions remain unchanged. This is one of the disadvantages of this method. Another problem is the determination of the value of the linear spring constant. Several methods proposed to estimate this value. Terzaghi [8] estimates these subgrade reaction methods as well as brief reviews of the practical application of subgrade reaction theories.

Other models were proposed to make the soil modeling more accurate from developments of the Winkler model by creating new parameters [9, 10]. These models, however, also suffer from the drawback that these parameters are difficult to determine. In recent years, a lot of research has been conducted in the field of soil-structure interaction, simulating the soil in a variety of complex ways based on Winkler.

Other branch of soil medium model is the elastic continuum model. It emerged with the analysis of conceptual physical problems used as the fundamental solution for other problems. The problem of determining the stress and displacement field in an isotropic half-space, which is acted upon by a concentrated point load on its surface (see figure 4). Boussinesq [11] was the first to use the continuum mechanics to model the soil as a semi-infinite, homogeneous, isotropic, linear elastic solid subjected to a concentrated force acting normal to the plane boundary. This approach provides much more information on the stresses and deformations within soil mass than the Winkler model. However, the drawback of this method is its complexity to be done computationally due to the appearance of improper integrals. Also, it was noticed an inaccuracy in reactions calculated at the peripheries of the foundation. In experimental observations the displacements of the surface away from the loaded region decreased more rapidly than what is predicted by this approach [12]. Several models have been developed as improved versions of the continuum model in view of mitigate these drawbacks.

Figure 4: Half-space acted upon by a normal point load on its surface.

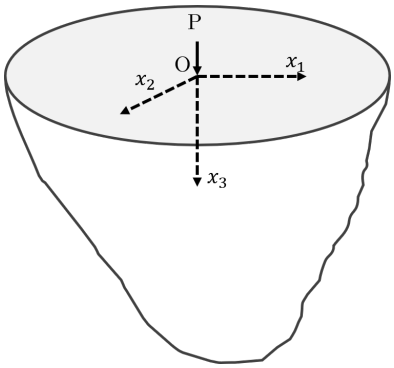

Diagram by Author.

Figure 5: FEM discreatization of the soil with an end-boundary.

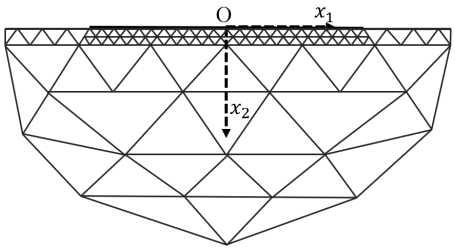

Diagram by Author.

The use of the FEM to model structures has been extensively studied since the seminal article by Turner *et al.*[13]. Since the number of elements to be used in any discretization is finite, even if millions of elements were used, soil would still have a boundary [14], see figure 5. Some works have tried to deal with this problem using a series of techniques. Godbole *et al.* [15] modeled the infinite extent of the soil domain with a coupled finite-infinite element formulation, to model the infinite extent of the soil domain. There are other ways to deal with this problem within the FEM, such as creating absorbent barriers, perfectly matched

layers, etc., but they also present challenges [6, 16].

The Boundary Element Method (BEM) is another popular numerical approach to geomechanical analysis used by a number of authors. Kokkinos and Spyrakos [17] used the BEM to model the elastic, isotropic, and homogeneous soil medium and FEM to model the flexible and massive foundation of a structure subjected to dynamic analysis. In a recent work, Barros *et al.* [18] proposed the soil modeling using the Indirect-BEM, and coupled a pile structure and foundation modeled via the FEM. The IBEM-FEM coupling scheme used in this dissertation uses the displacement influence functions available in the literature [19]. In addition, the formulations of the influence functions for the cases with a trench in the soil are given by Cortez *et al.* [20] who used a IBEM-FEM coupled formulation to model the soil and structure with the inclusion of a trench in the soil-structure interface.

Figure 6: BEM discreatization of the soil.

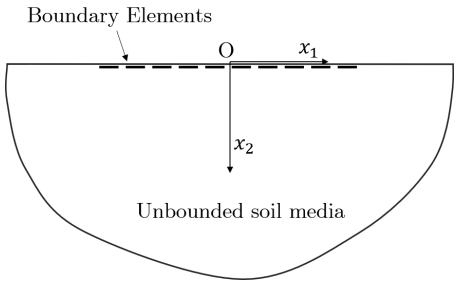

Diagram by Author.

2.2 Topology Optimization

2.2.1 Brief history of Optimization

Structural Optimization methods grew after the development of computational techniques that enabled the creation of algorithms based on theories already formulated by scholars in the 20th century. Figure 7 shows some results reached by Michell [21] in 1904 using the main isostress lines. The results essentially consisted of initially calculating the principal mechanical stress field, using the theory of elasticity, of a force applied at a point in an infinite domain that is subject to displacement constraints at other points. Once the main isostress lines were obtained, the basic idea was to propose in this domain a structure formed by bars (truss), in which each bar (truss element) was aligned with the main stress directions calculated in the domain [22]. Using these techniques enables more complex and non-intuitive solutions to emerge after the creating of computational tools.

Since the seminal article by Bendsøe and Kikuchi [24], optimization field has increased and several methods for solving topology optimization problems have been created. Depending on the values that design variables can assume, there are two main branches in topology optimization: the continuous density methods [23,25,26] and discrete (or binary) methods [4, 27–29]. Additionally, there are boundary description methods, such as the

Figure 7: Examples of truss structures obtained by Michell in 1904. The bars follow the main isotension lines.

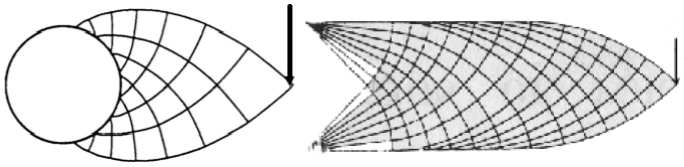

Adapted from Bendsøe and Sigmund [23].

ones based on level sets [30]. A review on topology optimization methods can be found in [31].

A famous example of continuous density methods is the *Solid Isotropic Material with Penalization* (SIMP) method created by Bendsøe and Sigmund [23, 26]. The acronym SIMP can denote both the optimization method and the material model, definition that will be presented later. It is sometimes called "material interpolation", "artificial material", "power law", or "density" method [32]. The SIMP method is one of the most widespread methods in TO because it is very versatile, it is widely accepted by the community, and it is able to solve various problems. As examples of problems that were solved in TO using SIMP we can mention: multiple load TO problems (Diaz and Bedsøe [33]), eigenvalue problem (Diaz e Kikuchi [34]), vibrating and design-dependent loads (Hammer and Olhoff [35] and Du e Olhoff [36]), and design of compliant mechanisms (solved by Sigmund [37]).

In addition, works on pressure loads such as the work of Sigmund and Clausen [38] have been developed, which suggested a new method to solve pressure load problems using a mixed displacement-pressure formulation for the finite element problem using SIMP. However, in continuous density methods applied to design-dependent pressure loads, challenges are in the identification of the structural boundaries or design-dependent loading during optimization. Wang *et al.* [39] propose a new material boundary identification scheme based on image segmentation technique to lead with this problem but still obtained gray scales final results. The article by Lundgaard *et al.* [40] applies the density-based topology optimization to fluid-structure-interaction problems using SIMP. Results have no clear boundary. So the author proposes the use of a penalty to lead to a discrete result. Furthermore, as soon as an element outside the fluid-structure interface is removed, instead of being replaced by an empty element, it is replaced by fluid.

More recently, authors have focused on proposing SIMP algorithms for solving optimization problems involving mechanical stress [41]. Du and Olhoff [42] discussed TO

involving natural frequency. Sigmund and Clausen [38] suggest a way to solve pressure load problems in TO using SIMP. Furthermore, geometrically nonlinear problems in optimization were also solved by Chen *et al.* [43] using density methods.

As examples of binary methods one has the *Evolutionary Structural Optimization* (ESO) method created by Xie and Steven [27], the most popular *Bi-directional Evolutionary Structural Optimization* (BESO) method presented by Huang and Xie [44], the Sequential Approximate Integer Programming with Trust-Region (SAIP-TP) method by Liang and Cheng [45] and the Topology Optimization of Binary Structures (TOBS) developed by Sivapuram and Picelli [4]. Several authors have proposed solutions to optimization problems using binary algorithms. Such as multi-material problems by Huang and Xie [46], vibration problems by Xie and Steven [47], mechanical stress [48] and nonlinearities [49]. Binary methods stand out for obtaining results with clear boundaries and have an advantage over design-dependent problems when compared to density methods. Picelli *et al.* [50] propose an evolutionary topology optimization method for compliance minimization of structures under design-dependent pressure loads. Problems with multiphysics interaction have also gained notoriety in recent years and are still an open problem in OT. Picelli *et al.* [51], solved TO for natural frequency maximization problems considering acoustic–structure interaction.

In addition to the types of methods discussed, there are also those based on boundary movement that mix topological optimization with shape optimization such as *The Level-Set Method* developed by Allaire *et al.* [30] that uses the level-set of a function to define the structural domain. The Level-set method is an example where a high-degree function is used to describe the structural domain boundary through its zero-value level-set function. Positive values represent the full structural domain and negative values the void structural domain, as shown in figure 8 from Deaton and Grandhi (2014)[31]. Such procedures use the position of the structural surfaces as design variables in order to keep track of the implicitly defined structural shapes. These methods can require fixed grids or remeshing, presenting special challenges in their numerical implementations.

The method of *Moving Morphable Components* (MMC) created by Zhang *et al.* [52] uses the position and size of predefined shapes to define the topology of the structure. Others methods are discussed in the references, see [31, 32] for an overview and classification.

Another famous solution to the topology optimization problem is the use of non-gradient based algorithms such as Genetic Algorithms [53], Ant Colonies, and others

Figure 8: The Level-Set Method domain representation.

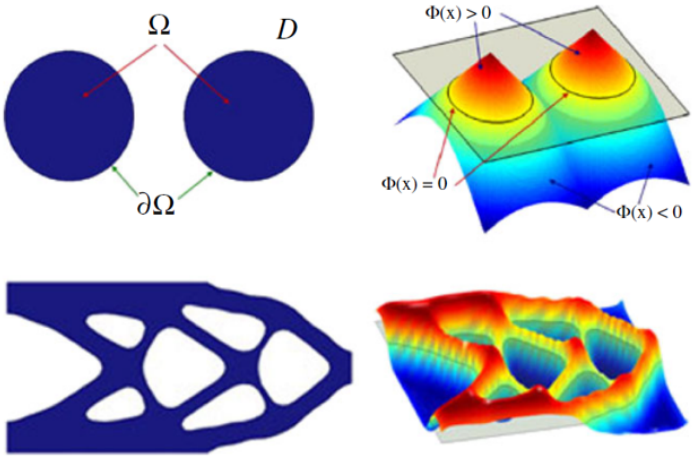

that use features of nature as a search engine in complex optimizable domains. However, Sigmund [54] showed that these non-gradient based techniques are inefficient in the context of optimization when compared with gradient based methods due to computational cost. Nonetheless, the usefulness of non-gradient based algorithms are in complex problems where gradient information is very hard to be computed [55].

2.3 Soil-Structure Interaction Topology Optimization

Into structural optimization context, the soil-structure iteration had recent contributions by Seitz and Grabe [56] who presented the TO of 3D structures for foundations in granular soil using the SIMP method. The authors limited to the design of foundations. Also, Tian *et al.* [57] explored the applicability of TO in structures on seabed also using SIMP. They modeled the soil using the Winkler model. Recently, Tavares and Labaki [58] used the BESO method to optimize structures on pilled foundations using a IBEM-FEM coupling. Siqueira *et al.* [59] also used the BESO method, optimized a tunnel reinforcement distribution topology. In their work, the unbounded soil was modeled using the IBEM and it was coupled with structure of the tunnel reinforcement modeled using the FEM.

Until the publication of this dissertation, the topology optimization of structures subjected to soil-structure iteration using the TOBS method and modeling the soil with IBEM was still unexplored. This work proposes to overcome this gap. This modeling allows the expansion of this analysis to dynamic, multi-objective and multi-material problems.

3 THEORETICAL FRAMEWORK

This chapter presents the theoretical foundation used in this dissertation. It presents the main ideas, concepts and important processes in the elasticity, soil modeling and optimization.

3.1 Linear Elasticity

Elasticity equations presented here govern both soil and structure domains. However, the solutions to the static problem for each of these coupled domains are achieved by different methods. It is important to state that it is generally convenient in soil mechanics to consider compressive stresses to be positive (see figure 9) meanwhile in the structure, normal stresses in the positive coordinate directions are positive. This difference in signals is taken into account at the soil-structure coupling step.

Figure 9: Infinitesimal 3D soil element.

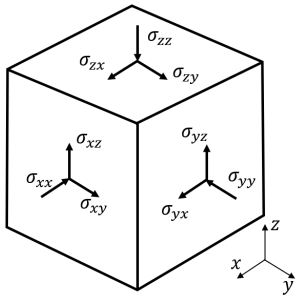

Diagram by Author.

Consider an infinitesimal 3D element as show in figure 9. The elastostatic equilibrium equations, in terms of stresses, in the absence of body forces, are

$$\frac{\partial \sigma_{xx}}{\partial x} + \frac{\partial \sigma_{xy}}{\partial y} + \frac{\partial \sigma_{xz}}{\partial z} = 0, \tag{3.1}$$

$$\frac{\partial \sigma_{xy}}{\partial x} + \frac{\partial \sigma_{yy}}{\partial y} + \frac{\partial \sigma_{yz}}{\partial z} = 0, \tag{3.2}$$

$$\frac{\partial \sigma_{zx}}{\partial x} + \frac{\partial \sigma_{zy}}{\partial y} + \frac{\partial \sigma_{zz}}{\partial z} = 0, \tag{3.3}$$

where, σ_{ij} are the stresses in the i face acting in the j-direction. If $i = j$, then σ_{ii} are normal stresses and when $i \neq j$, σ_{ij} are the shear stresses. $(i, j = x, y, z)$.

The theory of elasticity makes use of Hooke's law of elasticity as constitutive equation. Basically, bodies are considered elastic, that is, they deform linearly with the load and return to the initial state of inertia once the load is removed. This consideration is only true for small displacements. Hooke's law relates stress σ_{ij} to strain ε_{ij} using a constant

of elasticity. Considering the isotropy, strains are written as a function of the stresses as follows:

$$\varepsilon_{xx} = \frac{1}{E}[\sigma_{xx} - \nu(\sigma_{yy} + \sigma_{zz})], \tag{3.4}$$

$$\varepsilon_{yy} = \frac{1}{E}[\sigma_{yy} - \nu(\sigma_{xx} + \sigma_{zz})], \tag{3.5}$$

$$\varepsilon_{zz} = \frac{1}{E}[\sigma_{zz} - \nu(\sigma_{xx} + \sigma_{yy})], \tag{3.6}$$

$$\varepsilon_{xy} = \frac{1}{G}\sigma_{xy}, \tag{3.7}$$

$$\varepsilon_{yz} = \frac{1}{G}\sigma_{yz}, \tag{3.8}$$

$$\varepsilon_{zx} = \frac{1}{G}\sigma_{zx}, \tag{3.9}$$

in which, E is the Young's modulos, G the shear modulus and ν is the Poisson's ratio which relates the deformation (expansion or contraction) of a material in directions perpendicular to the specific direction of loading.

From equations 3.4 to 3.9, Hooke's law can be written in a matrix form as

$$\sigma = \mathbf{D}\varepsilon, \tag{3.10}$$

where σ is the stress tensor, ε the strain tensor and the matrix $\mathbf{D}$ for the elastic linear isotropic case is:

$$\mathbf{D} = \frac{E}{(1+\nu)(1-2\nu)} \begin{bmatrix} 1-\nu & \nu & \nu & 0 & 0 & 0 \\ \nu & 1-\nu & \nu & 0 & 0 & 0 \\ \nu & \nu & 1-\nu & 0 & 0 & 0 \\ 0 & 0 & 0 & \frac{(1-2\nu)}{2} & 0 & 0 \\ 0 & 0 & 0 & 0 & \frac{(1-2\nu)}{2} & 0 \\ 0 & 0 & 0 & 0 & 0 & \frac{(1-2\nu)}{2} \end{bmatrix}. \tag{3.11}$$

Since six strain components are derived from just three displacements, the strains are not independent of each other. Six additional relations, known as compatibility equations, can be derived. They are as follows:

$$\frac{\partial^2 \varepsilon_{xx}}{\partial y^2} + \frac{\partial^2 \varepsilon_{yy}}{\partial x^2} = \frac{\partial^2 \varepsilon_{xy}}{\partial x \partial y}, \tag{3.12}$$

$$\frac{\partial^2 \varepsilon_{yy}}{\partial z^2} + \frac{\partial^2 \varepsilon_{zz}}{\partial y^2} = \frac{\partial^2 \varepsilon_{yz}}{\partial y \partial z}, \tag{3.13}$$

$$\frac{\partial^2 \varepsilon_{zz}}{\partial x^2} + \frac{\partial^2 \varepsilon_{xx}}{\partial z^2} = \frac{\partial^2 \varepsilon_{xz}}{\partial x \partial z}, \tag{3.14}$$

$$2\left(\frac{\partial^2 \varepsilon_{xx}}{\partial y \partial x}\right) = \frac{\partial}{\partial x}\left(-\frac{\partial \varepsilon_{yz}}{\partial x} + \frac{\partial \varepsilon_{zx}}{\partial y} + \frac{\partial \varepsilon_{xy}}{\partial z}\right), \tag{3.15}$$

$$2\left(\frac{\partial^2 \varepsilon_{yy}}{\partial z \partial x}\right) = \frac{\partial}{\partial y}\left(\frac{\partial \varepsilon_{yz}}{\partial x} - \frac{\partial \varepsilon_{zx}}{\partial y} + \frac{\partial \varepsilon_{xy}}{\partial z}\right), \tag{3.16}$$

$$2\left(\frac{\partial^2 \varepsilon_{zz}}{\partial x \partial y}\right) = \frac{\partial}{\partial z}\left(\frac{\partial \varepsilon_{yz}}{\partial x} + \frac{\partial \varepsilon_{zx}}{\partial y} - \frac{\partial \varepsilon_{xy}}{\partial z}\right). \tag{3.17}$$

Considering the Hooke's law and strain-displacement relationships, the governing equations of elasticity, know as Navier's equations, are expressed in terms of displacements as

$$\mu \nabla^2 u_x + (\lambda + \mu)\frac{\partial e}{\partial x} = 0, \tag{3.18}$$

$$\mu \nabla^2 u_y + (\lambda + \mu)\frac{\partial e}{\partial y} = 0, \tag{3.19}$$

$$\mu \nabla^2 u_z + (\lambda + \mu)\frac{\partial e}{\partial z} = 0, \tag{3.20}$$

where $\nabla^2 = (\frac{\partial^2}{\partial x^2}\ \frac{\partial^2}{\partial y^2}\ \frac{\partial^2}{\partial z^2})$ is the Laplacian operator, $e = (\varepsilon_{xx} + \varepsilon_{yy} + \varepsilon_{zz})$ is the volumetric strain, and λ and μ are Lamé's constants defined as

$$\lambda = \frac{\nu E}{(1+\nu)(1-2\nu)} \quad and \quad \mu = \frac{E}{2(1+\nu)}. \tag{3.21}$$

Many situations in soil mechanics can be treated as two-dimensional problems in which only the stresses in a single plane need to be considered. The most important case is the plane strain in which the displacement in one of the coordinate directions (usually the y direction) is zero. In this case, the object have to be "long" in the y-direction. Another class of problems are those involving the plane stress where the stress at one of the coordinates (usually y) is zero. In this case, the thickness (measured in y) is very small, as in the case of thin plates.

Considering 2D analysis and the material as isotropic and homogeneous, one can write the equilibrium equation in terms of the displacement field $u_i = u_i(x, z)$ in the $i-$direction $(i = x, z)$ as

$$\alpha \frac{\partial^2 u_x}{\partial x^2} + \frac{\partial^2 u_x}{\partial z^2} + \kappa \frac{\partial^2 u_z}{\partial x \partial z} = 0, \tag{3.22}$$

$$\frac{\partial^2 u_z}{\partial x^2} + \alpha \frac{\partial^2 u_z}{\partial z^2} + \kappa \frac{\partial^2 u_x}{\partial x \partial z} = 0, \tag{3.23}$$

in which $\alpha = 2 + \lambda/\mu$, and $\kappa = 1 + \lambda/\mu$.

3.2 Soil Modeling

A number of approximations are used to model the soil depending on the level of rigor. In this dissertation soil is modeled as a elastic, continuous, homogeneous and isotropic medium, and the BEM is used to model the soil.

The BEM is a numerical method for solving boundary value problems (BVP) in engineering. Simply stated, a BVP is a mathematical problem in which one or more dependent variables must satisfy a differential equation everywhere within a known domain of independent variables and satisfy specific conditions on the boundary of the domain. The BEM is an alternative to the more traditional FEM. Moreover, this method is well-positioned in problems with infinite domains. The main feature of this method is that it is necessary to discretize only the boundary of the problem, in contrast to other methods, such as the FEM, that impose discretization of the entire domain. This feature makes the soil modeling using BEM attractive, being capable to model an 3D infinite soil by discretizating only the 2D soil-structure interface. There is a decrease in the discretized dimension. Also, the BEM provides very good accuracy, especially away from the boundaries whereas the FEM provides exact solutions only at nodal points.

Some of the disadvantages of the BEM are: Matrix to be solved is full and asymmetric; its conditioning is not always very good; evaluating the singular integrals on the boundaries can be difficult; there are a number of singularities and improper integrals that must be computed numerically. Some of these problems can be solved using numerical integration techniques and applying it to well-posed problems.

There are two common branches of the BEM: these are known as the so called direct and indirect formulations. The main difference between the two formulations is the use of continuous variables with physical meaning (the direct formulation) or the use of unknown functions represented by fictitious source densities that are used later to calculate real variables of the problem (the indirect formulation)[60].

The BEM is indicated for problems that have a small boundary/volume ratio, which is the case of infinite soil. Therefore, it is recommended in the literature [17] to use the BEM to model the soil medium and the FEM to model the structure. These two different idealization methods can be appropriately matched at the interface through balance and compatibility conditions.

3.2.1 Solution strategy

BEM is based on finding the solution for the displacement (and tension) of the domain from the principle of superposition of displacements caused by loads applied in specific regions of the space. The solutions for the influence of these loads in space are called fundamental solutions. These solutions are only available for relatively simple types of loading. These solutions are usually found in the literature in the form of functions and tables.

The solutions for the surface loading cases studied in this dissertation are found in [19] and the solutions for the influence functions for the buried loading case used in this dissertation are found in [20]. The derivation consists in subjecting the coupled equilibrium equations of soil media to a Fourier transformation, in the space of which boundary conditions corresponding to buried loads can be imposed algebraically. Stress fields are obtained from their displacements counterparts through the constitutive equation (see equations 3.4 to 3.9). Final solutions for the stress and displacement fields of the soil are expressed in terms of improper integrals in the Fourier transformed space, and must be evaluated numerically to obtain the solutions in the physical space.

The linear system of equations in Eqs. 3.22 and 3.23 can be written in matrix form as

$$\begin{bmatrix} \alpha\frac{\partial^2}{\partial x^2} + \frac{\partial^2}{\partial z^2} & \kappa\frac{\partial^2}{\partial x\,\partial z} \\ \kappa\frac{\partial^2}{\partial x\,\partial z} & \frac{\partial^2}{\partial x^2} + \alpha\frac{\partial^2}{\partial z^2} \end{bmatrix} \begin{Bmatrix} u_x \\ u_z \end{Bmatrix} = \mathbf{Lu} = \mathbf{0}. \tag{3.24}$$

The non-trivial solution for this matrix equation is obtained when $\det \mathbf{L} = 0$, which yields

$$\alpha\frac{\partial^4 u_i}{\partial x^4} + \alpha\frac{\partial^4 u_i}{\partial z^4} + \gamma\frac{\partial^4 u_i}{\partial x^2 \partial z^2} = 0, \tag{3.25}$$

in which $\gamma = 4 + 2\lambda/\mu$ and $i = (x, z)$. Applying a Fourier transformation to equation 3.25 yields the uncoupled set of equations

$$\alpha\zeta^4\bar{u}_i + \alpha\frac{\partial^4 \bar{u}_i}{\partial z^4} - \gamma\zeta^2\frac{\partial^2 \bar{u}_i}{\partial z^2} = 0, \tag{3.26}$$

in which ζ is the Fourier space variable, and the bar on top of variables indicates that they are written in the transformed space. Assuming that $\bar{u_z}$ is of the form $\bar{u_z} = \mathrm{e}^{\xi z} \neq 0$, it comes from equation 3.26 that $\alpha\zeta^4 + \alpha\xi^4 - \gamma\zeta^2\xi^2 = 0$, which has the following four roots: $\pm\xi_i$ $(i = 1, 2)$ such that

$$\xi_{1,2} = \frac{\sqrt{\gamma\zeta^2 \pm \sqrt{\Phi}}}{\sqrt{2\alpha}}, \tag{3.27}$$

in which $\Phi = \gamma^2 - 4\alpha^2$. General solutions for u_i can be obtained following the form above as

$$\bar{u_x} = \bar{\omega}_1 A e^{-\xi_1 z} - \bar{\omega}_1 B e^{\xi_1 z} + \bar{\omega}_2 C e^{-\xi_2 z} - \bar{\omega}_2 D e^{\xi_2 z}, \tag{3.28}$$

$$\bar{u_z} = A e^{-\xi_1 z} + B e^{\xi_1 z} + C e^{-\xi_2 z} + D e^{\xi_2 z}, \tag{3.29}$$

with

$$\bar{\omega}_i = \frac{\alpha \xi_i^2 - \zeta^2}{i \kappa \zeta \xi_i},$$

in which the exponential terms are selected so that the general expression complies with Sommerfeld's radiation condition for $z \to \pm\infty$ [61], and A, B, C, and D are arbitrary functions to be determined from the boundary conditions of a given problem.

3.2.2 Stress fields

The infinitesimal strain components in this two-dimensional, plane strain problem are given by $\varepsilon_{ij} = (u_{i,j} + u_{j,i})/2$, $(i, j = x, z)$, and the constitutive equation is $\sigma_{ij} = \lambda (\nabla \bullet \mathbf{u}) \delta_{ij} + \mu (u_{i,j} + u_{j,i})$, with $\mathbf{u} = \left\{ \begin{array}{cc} u_x & u_z \end{array} \right\}^T$, in which δ_{ij} is the Krönecker delta. In view of Eqs. 3.28 and 3.29, general expression for the stress components in the Fourier transformed space can be written as

$$\bar{\sigma}_{xx} = \mu \left(\eta_1 A e^{-\xi_1 z} - \eta_1 B e^{\xi_1 z} + \eta_2 C e^{-\xi_2 z} - \eta_2 D e^{\xi_2 z} \right), \tag{3.30}$$

$$\bar{\sigma}_{xz} = \mu \left(\eta_3 A e^{-\xi_1 z} + \eta_3 B e^{\xi_1 z} + \eta_4 C e^{-\xi_2 z} + \eta_4 D e^{\xi_2 z} \right), \tag{3.31}$$

$$\bar{\sigma}_{zz} = \mu \left(\eta_5 A e^{-\xi_1 z} - \eta_5 B e^{\xi_1 z} + \eta_6 C e^{-\xi_2 z} - \eta_6 D e^{\xi_2 z} \right), \tag{3.32}$$

in which

$$\eta_{1,2} = \frac{1}{\kappa \xi_{1,2}} \left[\left(\alpha^2 - \kappa^2 + \kappa \right) \xi_{1,2}^2 - \zeta^2 \alpha \right],$$

$$\eta_{3,4} = \frac{i}{\kappa \zeta} \left[\alpha \xi_{1,2}^2 + (\kappa - 1) \zeta^2 \right],$$

$$\eta_{5,6} = -\frac{1}{\kappa \xi_{1,2}} \left[(\kappa - 1) \zeta^2 + \alpha \xi_{1,2}^2 \right].$$

3.2.3 General solution

Equations 3.28 to 3.32 express general displacement and stress fields in the Fourier transformed space ζ. Their physical-domain (x, z) counterparts are obtained upon subjecting them to inverse Fourier transforms, which results in

$$u_x = \frac{1}{\sqrt{2\pi}} \int_{-\infty}^{\infty} \left(\bar{\omega}_1 A e^{-\xi_1 z} - \bar{\omega}_1 B e^{\xi_1 z} + \bar{\omega}_2 C e^{-\xi_2 z} - \bar{\omega}_2 D e^{\xi_2 z} \right) e^{i \zeta x} d\zeta, \tag{3.33}$$

$$u_z = \frac{1}{\sqrt{2\pi}} \int_{-\infty}^{\infty} \left(Ae^{-\xi_1 z} + Be^{\xi_1 z} + Ce^{-\xi_2 z} + De^{\xi_2 z} \right) e^{i\zeta x} d\zeta, \tag{3.34}$$

$$\sigma_{xx} = \frac{\mu}{\sqrt{2\pi}} \int_{-\infty}^{\infty} \left(\eta_1 Ae^{-\xi_1 z} - \eta_1 Be^{\xi_1 z} + \eta_2 Ce^{-\xi_2 z} - \eta_2 De^{\xi_2 z} \right) e^{i\zeta x} d\zeta, \tag{3.35}$$

$$\sigma_{xz} = \frac{\mu}{\sqrt{2\pi}} \int_{-\infty}^{\infty} \left(\eta_3 Ae^{-\xi_1 z} + \eta_3 Be^{\xi_1 z} + \eta_4 Ce^{-\xi_2 z} + \eta_4 De^{\xi_2 z} \right) e^{i\zeta x} d\zeta, \tag{3.36}$$

$$\sigma_{zz} = \frac{\mu}{\sqrt{2\pi}} \int_{-\infty}^{\infty} \left(\eta_5 Ae^{-\xi_1 z} - \eta_5 Be^{\xi_1 z} + \eta_6 Ce^{-\xi_2 z} - \eta_6 De^{\xi_2 z} \right) e^{i\zeta x} d\zeta, \tag{3.37}$$

in which A, B, C, and D depend on particular boundary-value problems.

3.2.4 BVP: layer over rigid base

In this dissertation, we obtain the displacement and stress fields for the BVP of a soil layer of depth h resting over a rigid base. This is the soil medium considered in one of the results that presents a canal.

The layer is divided into media 1 ($0 < z < z'$) and 2 ($z' < z < h$), at the interface of which ($x = x', z = z'$) a point load $p_i(x, z) = \delta(x', z')$ is applied. The index $i = x, z$ denote the direction of the load and δ is the Dirac Delta. The expression for p_i in the Fourier space is $\bar{p}(\zeta) = (2\pi)^{-1}$.

Continuity conditions are imposed at the interface between media (1) and (2), $u_i^{(1)}(x, z') = u_i^{(2)}(x, z')$, in which the superindices denote the media referred to by u_i. The free surface of the layer is described by imposing that $\sigma_{ij}^{(1)}(x, z = 0) = 0$. The presence of the rigid base is described by imposing that $u_i^{(2)}(x, h) = 0$. For horizontal loads, equilibrium conditions are imposed as $\sigma_{xz}^{(1)}(x, z') - \sigma_{xz}^{(2)}(x, z') = p_x(x, z')$ and $\sigma_{zz}^{(1)}(x, z') - \sigma_{zz}^{(2)}(x, z') = 0$, and for vertical loads $\sigma_{xz}^{(1)}(x, z') - \sigma_{xz}^{(2)}(x, z') = 0$ and $\sigma_{zz}^{(1)}(x, z') - \sigma_{zz}^{(2)}(x, z') = p_z(x, z')$.

In order to formulate the constant boundary elements used to model the soil in this dissertation, stress and displacement fields due to uniformly distributed buried loads must be derived. These are extensions of the BVP above for the case in which the point load is replaced by loads that are distributed on a horizontal or vertical line of length $2a$. These can be written as $p_i(x, z) = H(-a) - H(a)$, in which H is the unit Heaviside step distribution, and their expression in the Fourier space is $\bar{p}(\zeta) = 2\sin(\zeta a)/\sqrt{2\pi}\zeta$. The corresponding boundary conditions must be imposed for $-a < x < a$, $z = z'$ for horizontally-distributed loads, and for $-a < z' < a$, $x = x'$ for the case of vertically-distributed loads. Horizontally- and vertically-distributed loads are used in this dissertation to describe respectively the bottom and side faces of the canal.

3.2.5 Isotropic layer case

A crucial detail for the isotropic layer case considered in this dissertation is that, in this case, $\Phi = 0$ and $\xi_1 = \xi_2 = \zeta$ (equation 3.27), and the numerical evaluation of Eqs. 3.33–3.37 is sometimes unattainable. A special solution has been derived for this case, with the introduction of variable

$$\theta = \frac{\lambda}{\mu} = \frac{2\nu}{1-2\nu}, \tag{3.38}$$

in which ν is the Poisson ratio. In view of equation 3.38, $\alpha = \theta + 2$ and $\kappa = \theta + 1$, and displacement and stress solutions for the isotropic case can be written as

$$\bar{u_x}(\zeta, z) = Ae^{-\zeta z} + Be^{\zeta z} + \omega_1 Ce^{-\zeta z} + \omega_2 De^{\zeta z},$$

$$\bar{u_z}(\zeta, z) = iAe^{-\zeta z} - iBe^{\zeta z} + i\zeta z Ce^{-\zeta z} - i\zeta z De^{\zeta z},$$

$$\bar{\sigma}_{xx}(\zeta, z) = \mu(2i\zeta Ae^{-\zeta z} + 2i\zeta Be^{\zeta z} + 2i\zeta\eta_1 Ce^{-\zeta z} + 2i\zeta\eta_2 De^{\zeta z}),$$

$$\bar{\sigma}_{xz}(\zeta, z) = \mu(-2\zeta Ae^{-\lambda z} + 2\zeta Be^{\zeta z} - 2\zeta\eta_3 Ce^{-\zeta z} + 2\zeta\eta_4 De^{\zeta z}),$$

$$\bar{\sigma}_{zz}(\zeta, z) = \mu(-2i\zeta Ae^{-\lambda z} - 2i\zeta Be^{\zeta z} - 2i\zeta\eta_5 Ce^{-\zeta z} - 2i\zeta\eta_6 De^{\zeta z}),$$

in which

$$\omega_{1,2} = \zeta z \mp \frac{\theta+3}{\theta+1},$$

$$\eta_{1,2} = \zeta z \mp \frac{2\theta+3}{\theta+1},$$

$$\eta_{3,4} = \zeta z \mp \frac{\theta+2}{\theta+1},$$

$$\eta_{5,6} = \zeta z \mp \frac{1}{\theta+1}.$$

3.2.6 Numerical evaluation

The numerical evaluation of Eqs. 3.33–3.37 requires special attention. The integrand of these expressions contain a number of singularities within $0 < \zeta \leq 1$, and an indefinitely alternating-decaying behavior for $\zeta > 1$. In the present implementation, we incorporate a small damping η into μ through $\mu^* = \mu\,(1 + i\eta)$ [62] and use the complex-valued μ^* instead of μ throughout the analysis. This has negligible effect in the response of the soil, but it takes the singularities out of the real contour of integration, and makes the evaluation of the integral possible through some classical adaptive Gaussian quadrature [63]. For the $\zeta > 1$ domain, we use an extrapolation-based numerical recipe that avoids

truncation of the integration interval [64].

3.3 Finite Element Method Modeling

The finite element method, sometimes referred to as finite element analysis (FEA), is a computational technique used to obtain approximate solutions of BVP in engineering. The idea is to divide the domain of the continuous structure into smaller discrete structures called elements. The equilibrium equation of the full structure is given by:

$$\mathbf{Ku} = \mathbf{F}, \tag{3.39}$$

where $\mathbf{K}$ is the global stiffness matrix, $\mathbf{u}$ is the displacement field and $\mathbf{F}$ is the vector of forces. The balance of the structure is resolved within each element and then assembled on the full structure to obtain an approximate solution.

The number of elements used to discretize the domain defines the desired level of approximation to the final solution. The more elements used, the better the approximation. When more elements are used, the discretization is said to be more refined. Figure 10 shows two modeling examples using elements of different sizes. The shaded region represents the area not included in the model. This area is smaller when the discretization is more refined. The elements of a discretization are interconnected by nodes. The solution is given at each node and interpolated throughout the element.

Figure 10: Arbitrary shape geometry modeled using square elements. a) Using 16 finite elements the area not included in the model is larger than b) using 85 elements.

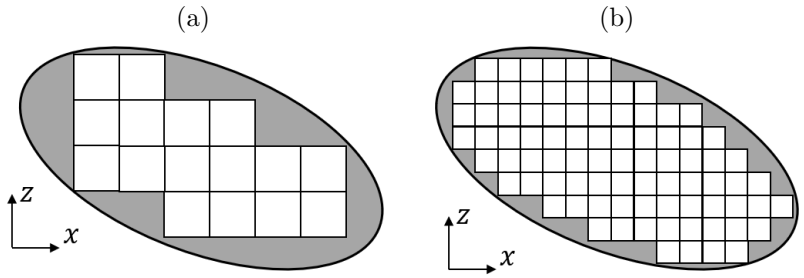

Illustration by Author.

Depending on the type of element used, approximations to the displacement are defined for the equilibrium equation solution. These answers are approximated using so-called shape functions N_i as:

$$\bar{\mathbf{u}} = \sum_{i=1}^{4} \mathbf{N_i u_i}. \tag{3.40}$$

where $\bar{\mathbf{u}}$ is the approximated displacement field and $\mathbf{u_i}$ the displacements at each node i.

Figure 11: Quadrilateral element.

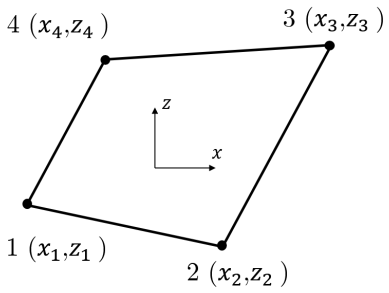

Illustration by Author.

In this dissertation, the structure is discretized using a two-dimensional isoparametric quadrilateral element as shown in the figure 11. The shape functions for interpolate displacement are given by:

$$\begin{aligned} N_1 &= 1/4(1-r)(1-s) \\ N_2 &= 1/4(1+r)(1-s) \\ N_3 &= 1/4(1+r)(1+s) \\ N_4 &= 1/4(1-r)(1+s) \end{aligned} \tag{3.41}$$

where r and s are the local coordinates of the parent element as shown in the figure 12.

The quadrilateral element is a 4-noded element and has 2 degree of freedom (DOF) per node. Isoparametric element uses a mapping scheme to deal with deformed elements. In this approach, each node is related to a rectangular parent element in a regular discretization as the illustration in the figure 12. An interpolation function is used to map the element. The geometry interpolation is given by:

$$\mathbf{x} = \sum_{i=1}^{4} \mathbf{N_i x_i}, \tag{3.42}$$

where $\mathbf{N_i}$ are the same shape functions used to interpolate the displacement shown in equations 3.41.

Figure 12: Mapping of isoparametric element geometry.

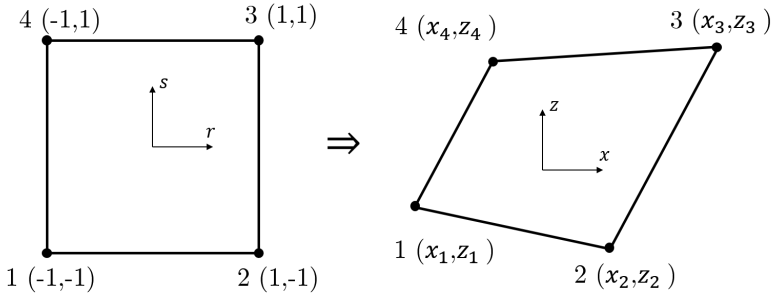

Illustration by Author.

Once the mapping is done, we can write the local coordinates r and s as a function of the global coordinates x and z. Deriving the displacement (u or v) in relation to the

global coordinates and using the chain rule, one has

$$\begin{aligned}\frac{\partial()}{\partial r} &= \frac{\partial()}{\partial x}\frac{\partial x}{\partial r} + \frac{\partial()}{\partial z}\frac{\partial z}{\partial r} \\ \frac{\partial()}{\partial s} &= \frac{\partial()}{\partial x}\frac{\partial x}{\partial s} + \frac{\partial()}{\partial z}\frac{\partial z}{\partial s},\end{aligned} \tag{3.43}$$

and then one can write

$$\begin{Bmatrix} \dfrac{\partial()}{\partial r} \\ \\ \dfrac{\partial()}{\partial s} \end{Bmatrix} = \begin{bmatrix} \dfrac{\partial x}{\partial r} & \dfrac{\partial z}{\partial r} \\ \\ \dfrac{\partial x}{\partial s} & \dfrac{\partial z}{\partial s} \end{bmatrix} \begin{Bmatrix} \dfrac{\partial()}{\partial x} \\ \\ \dfrac{\partial()}{\partial z} \end{Bmatrix} \Rightarrow \begin{Bmatrix} \dfrac{\partial()}{\partial r} \\ \\ \dfrac{\partial()}{\partial s} \end{Bmatrix} = [\mathbf{J}] \begin{Bmatrix} \dfrac{\partial()}{\partial x} \\ \\ \dfrac{\partial()}{\partial z} \end{Bmatrix}, \tag{3.44}$$

in which $\mathbf{J}$ is the Jacobian matrix.

The deformations in the elements are defined from the derivatives of the displacements with respect to local coordinates:

$$\varepsilon = \mathbf{Bu} \tag{3.45}$$

where the matrix $\mathbf{B}$ is obtained by differentiating the shape functions $\mathbf{N}$.

The element stiffness matrix $\mathbf{K_e}$ is given by

$$\mathbf{K_e} = \int_V \mathbf{B}^T\mathbf{DB}dV \tag{3.46}$$

where V denotes the volume. The integration is done numerically using the Gaussian integration. For this, it is convenient to transform the limits of integration as follows

$$\mathbf{K_e} = \int_{-1}^{1}\int_{-1}^{1} \mathbf{B}^T\mathbf{DB}t\ det(\mathbf{J})drds \tag{3.47}$$

considering a constant thickness t.

A set of 2x2 points are used to calculate the Gaussian quadrature. Structural displacements are evaluated at the nodes and stress are calculated at the centroid of the element. Figure (13) shows a representative element with the Gauss points used to calculate displacements and stress calculations.

Once the element stiffness matrix is calculated, the global stiffness matrix is assembled. Boundary conditions are given by coupling with the soil, as presented in the Methodology section.

Figure 13: Gaussian quadrature points for calculating a) displacements and b) stresses.

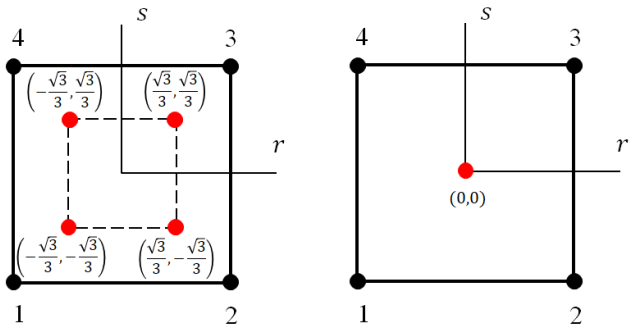

Illustration by Author.

3.4 Optimization

Optimization refers to strategies for a rationalized search for an optimal solution automatically, systematically and independent of the designer's experience. A well-known example is maximizing a company's profit given the products it can produce, restricted to the amount of raw material available. For an inattentive reader, this problem may seem simple, it would be enough to analyze all the options and choose the best one. However, real-world problems can have thousands of variables and millions of combinations.The smartest way to find the optimum is to analyze by performance by using Operational Research.

Operational Research (OR) is the search for the best use of resources and processes to improve decision-making of a real problem. It is sometimes defined as the search for methods to determine extreme values (maximum or minimum) of a function (profit, performance, cost, loss). It is done by manipulating variables under constraint conditions. By using other mathematical science fields such as modeling, statistics, and optimization, OR arrives at the optimal or near-optimal solution to complex decision problems.

Optimization is a field of mathematics. It is also called *mathematical programming*, "a somewhat confusing term coined in the 1940s, before the word "programming" became inseparably linked with computer software" [65]. The development of mathematical programming in the 1940s stimulated the field and led to the publication of several articles and books in addition to the creation and investigation of new optimization methods.

3.4.1 Fundamentals of Optimization

In the 1960s, with the emergence of the FEM, structural optimization problems began to be widely studied and applied in engineering, mainly in the aeronautical industry, where weight restrictions are more important than cost restrictions. The idea of developing a structure with greater stiffness and with as little material as possible can be achieved by minimizing the *Structural Mean Compliance*, subjecting the structural domain to a volume constraint. *Structural Mean Compliance* ($\boldsymbol{C}$) is a scalar quantity that can be understood as the inverse of structural stiffness. This property is given by the work of a applied external force $\boldsymbol{F}$ that generates a displacement $\boldsymbol{U}$ in the structure.

$$\boldsymbol{C} = \frac{1}{2}\boldsymbol{F}^T\boldsymbol{U}. \tag{3.48}$$

Generally speaking, the smaller the *compliance* of a structure, the greater its *stiffness*. Many algorithms in topology optimization work on minimize the *compliance* of a structure, subject to a volume constraint, thus maximizing the structural stiffness given a final volume constraint. In this dissertation, all problems are of compliance minimization.

Some concepts that are fundamental within the field of optimization are *design variables*, *objective function* and *constraint function* are introduced bellow:

- Design variables: are the variables that the designer has control. The determination of their value is the goal of the optimization process. They are usually presented in the form of a $\mathbf{x}$ vector. Example: quantity of products of type "A" or "B" to be produced, the values to be invested in each investment, cross-sectional area, member sizes, where there will be or not material in a structure, etc.

- Objective functions: these are functions to be extremized that depend on the design variable. Some problems that can have multiple objective functions are called multi-objective. Examples in classical problems are cost to be minimized, profit to be maximized, minimization of compliance, etc.

- Constraint functions: are functions that constrain the domain to a region of interest in which the problem is delimited. They can be of two types: inequality when delivering upper and/or lower bounds to the design variable or equality which are more restrictive, as they encircle the viable domain more tightly. Examples include the restriction of expenses, material, volume, etc. Constraint functions define the *viable domain*: the domain location where all constraint functions are satisfied. Within this domain there is an extreme value that is the best answer to the problem.

Optimization methods try to reach this point although there is no guarantee that they will have reached it at the end of the optimization.

The values that design variables can take are often used as a way of classifying optimization methods. Depending on the problem to be addressed, each optimization method, or the choice of design variable, can bring advantages and disadvantages.

Within Linear Programming (LP), for problems in which design variables can only assume integer values, the problems are said to be of *Integer Linear Programming* (ILP). When the variables can only assume values 0 or 1 we call it *Binary Variables*. Finally, *Mixed Integer Linear Programming* (MILP) are those where some design variables can be continuous and other can assume only integer values.[22]

In the context of structural optimization the term "Binary Structures" can denotes structures whose domain can be defined by 0 for void locations or 1 to solid locations. "Binary methods" make use of this property. This has a number of advantages when compared to other ways of defining design variables. Some of these advantages are easier problem boundary definition, ability to deal with multi-physics and multi-objective problems, etc.

3.4.1.1 Standard Formulation

Optimization problems can be written as follows

$$\begin{aligned} &\underset{x}{\text{Minimize}} && f(x) \\ &\text{subject to} && g(x) \leq 0, \\ & && h(x) = 0, \\ & && x \in \Omega_x \end{aligned} \tag{3.49}$$

where $f(x)$ is the objective function to be extremized, $g(x)$ are inequality constraint functions, $h(x)$ equality constraint functions and x is the vector of design variables that belong to a domain Ω_x. The values of x that satisfy the constraints form the feasible domain. Using minimization as the default in the notation does not generate a loss of generality since we can switch to a maximization problem just by changing the sign of f(x) to negative.

When both the objective function and constraint functions are linear functions of design variable so the problems are of linear optimization and are solved by *Linear Programming* (LP). However, if at least one of this functions is a nonlinear function of design

variable, so the problems is said to be of nonlinear optimization and make use of *Nonlinear Programming* (NLP).

3.4.2 Structural Optimization

Optimization of structures can take place along three lines [22]: Parametric Optimization, Shape Optimization and Topology Optimization. Figure 14 shows examples of the three categories of optimization.

Figure 14: Three categories of structural optimization. Parametric Optimization, Shape Optimization and Topology Optimization.

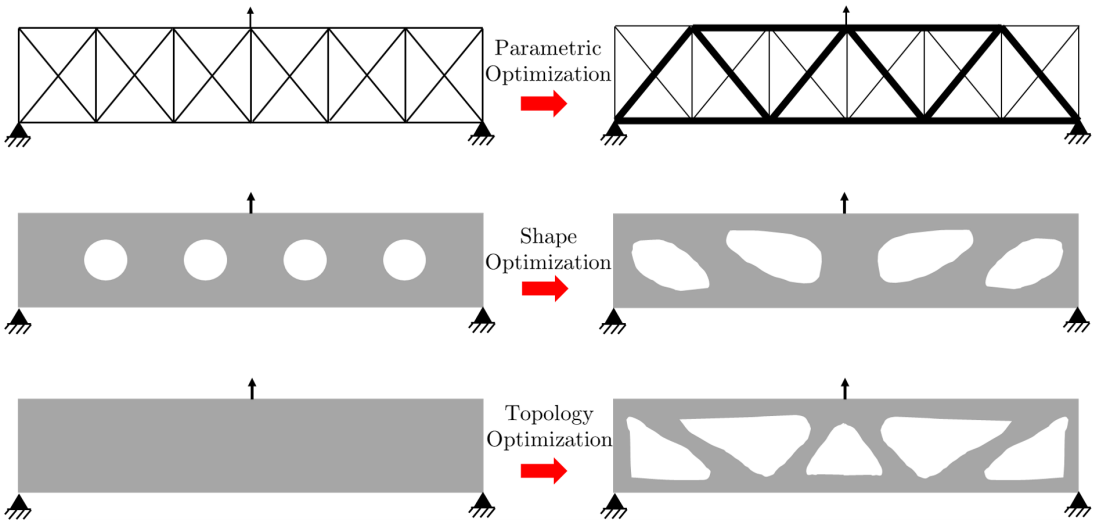

- Parametric Optimization: an initial shape of the structure is given, based on the designer's experience and the structure parameters are optimized, such as diameters, lengths, thicknesses, etc., subject to a constraint such as local stress, deflection, etc.

- Shape Optimization: in shape optimization, an initial topology is given (Initial shape with location and number of holes) and then the shape of the structure boundaries and holes are optimized without modifying their topology (number of holes and bars) generally using spline curves. In this type of optimization new holes does not appear.

- Topology Optimization: the material distribution over a solid domain is controlled by a design variable. The process consists of defining in the optimized structure where the material is present (design variable equals to 1) or absent (design variable equals to 0).

3.4.3 Sensitivity Analysis

Sensitivities are numerical evaluations of how the function of some variable changes due to a change in the design variable. Objective and constraint functions must be evaluated at each optimization step for their sensitivity when the design variable changes. This can be done via the derivatives of these functions.

Between the main method for calculating the sensitivities of a function, one can cite: Finite Difference Method (FDM), Analytical Methods and the Semi-Analytical Method. The choice of method to use depends on the number of design variables $\boldsymbol{n}$ and the number of constraints $\boldsymbol{n_i}$, although this choice can also be up to the programmer.

3.4.3.1 Finite Difference Method

The FDM is an easy to implement and very popular method that can be divided into: progressive, regressive or central difference method [66].

In progressive finite difference, having in hand the value of the function in x_i, the function is evaluated at a point $x_i + \Delta x$ and a linear approximation of the derivative is made as follows:

$$\frac{df(\boldsymbol{x})}{dx_i} = \frac{f(x_i + \Delta x) - f(x_i)}{\Delta x}, \tag{3.50}$$

where $\boldsymbol{n}$ additional analysis are needed to calculate $f(x_i + \Delta x)$ and the estimated approximation error is on the order of Δx.

In the regressive FDM, having the value of the function in x_i, the function is evaluated at a point $x_i - \Delta x$ and a linear approximation of the derivative is made as follows:

$$\frac{df(\boldsymbol{x})}{dx_i} = \frac{f(x_i) - f(x_i - \Delta x)}{\Delta x}, \tag{3.51}$$

here again, $\boldsymbol{n}$ additional analysis are needed to calculate $f(x_i - \Delta x)$ and the estimated approximation error is on the order of Δx.

Finally, in the central finite difference, the function is calculated at an earlier point $f(x_i - \Delta x)$ and a later point $f(x_i + \Delta x)$ in order to make use of a linear approximation of the derivative as follows

$$\frac{df(\boldsymbol{x})}{dx_i} = \frac{f(x_i + \Delta x) - f(x_i - \Delta x)}{\Delta x}, \tag{3.52}$$

where $2\boldsymbol{n}$ additional analysis is needed to calculate $f(x_i - \Delta x)$ and $f(x_i + \Delta x)$ and the estimated approximation error is on the order of Δx^2. That is, it is more expensive than

the progressive and regressive methods, but more accurate.

3.4.3.2 Analytical Methods

Among the methods for calculating sensitivity, the analytical method is the most accurate. It provides the exact value. It is based on numerical calculus theory and uses differentiation rules like chain rule, and product rule, etc. [66].

The analytical method can be divided into direct method or adjunct method.

- **Direct Method**

Let an objective function $f(\boldsymbol{u}(\boldsymbol{x}), \boldsymbol{x})$ with a constraint of the type $\boldsymbol{A}(\boldsymbol{x})\boldsymbol{u} = \boldsymbol{B}(\boldsymbol{x})$, one has for the direct method:

$$\frac{df(\boldsymbol{u}, \boldsymbol{x})}{d\boldsymbol{x}} = \frac{\partial f(\boldsymbol{u}, \boldsymbol{x})}{\partial \boldsymbol{x}} + z^T \frac{d\boldsymbol{u}}{d\boldsymbol{x}}, \tag{3.53}$$

where the first term is the explicit derivative (usually zero), the second term is the implicit derivative calculated using the chain rule, and z is the gradient of f with respect to $\boldsymbol{u}(\boldsymbol{x})$

$$z = \nabla_u f. \tag{3.54}$$

The derivative $d\boldsymbol{u}/d\boldsymbol{x}$ in the last term of equation 3.53 can be calculated from the constraint:

$$\begin{gathered} \boldsymbol{A}(\boldsymbol{x})\boldsymbol{u} = \boldsymbol{B}(\boldsymbol{x}) \\ \Rightarrow \frac{d(\boldsymbol{A}(\boldsymbol{x})\boldsymbol{u})}{d\boldsymbol{x}} = \frac{d\boldsymbol{B}(\boldsymbol{x})}{d\boldsymbol{x}}, \end{gathered} \tag{3.55}$$

applying the product rule on the left side of the equality we can rewrite

$$\frac{d\boldsymbol{A}(\boldsymbol{x})}{d\boldsymbol{x}}\boldsymbol{u} + \boldsymbol{A}(\boldsymbol{x})\frac{d\boldsymbol{u}}{d\boldsymbol{x}} = \frac{d\boldsymbol{B}(\boldsymbol{x})}{d\boldsymbol{x}}, \tag{3.56}$$

isolating the term $d\boldsymbol{u}/d\boldsymbol{x}$, we have

$$\frac{d\boldsymbol{u}}{d\boldsymbol{x}} = \boldsymbol{A}^{-1}(\boldsymbol{x}) \left(\frac{d\boldsymbol{B}(\boldsymbol{x})}{d\boldsymbol{x}} - \frac{d\boldsymbol{A}(\boldsymbol{x})}{d\boldsymbol{x}}\boldsymbol{u} \right), \tag{3.57}$$

the above system must be resolved for each design variable $\boldsymbol{x}$. Therefore, we can write the sensitivity as:

$$\frac{df(\boldsymbol{u}, \boldsymbol{x})}{d\boldsymbol{x}} = \frac{\partial f(\boldsymbol{u}, \boldsymbol{x})}{\partial \boldsymbol{x}} + z^T \boldsymbol{A}^{-1}(\boldsymbol{x}) \left(\frac{d\boldsymbol{B}(\boldsymbol{x})}{d\boldsymbol{x}} - \frac{d\boldsymbol{A}(\boldsymbol{x})}{d\boldsymbol{x}}\boldsymbol{u} \right), \tag{3.58}$$

the matrices $\boldsymbol{A}(x)$ and $\boldsymbol{B}(x)$ can usually be written explicitly in terms of $\boldsymbol{x}$ and their derivatives are computed analytically.

- **The Adjoint Method**

Consider an objective function $f(\boldsymbol{u}(\boldsymbol{x}), \boldsymbol{x})$ with a constraint of the type $\boldsymbol{A}(\boldsymbol{x})\boldsymbol{u} = \boldsymbol{B}(\boldsymbol{x})$, one has for the adjunct method:

$$L(\boldsymbol{u}(\boldsymbol{x}), \boldsymbol{x}, \lambda) = f(\boldsymbol{u}(\boldsymbol{x}), \boldsymbol{x}) + \lambda^T(\boldsymbol{A}(\boldsymbol{x})\boldsymbol{u} - \boldsymbol{B}(\boldsymbol{x})), \tag{3.59}$$

where λ is an arbitrary variable called adjoint variable. With respect to the restriction, the second term on the right side of the equation is null, so

$$\frac{dL}{d\boldsymbol{x}} = \frac{df}{d\boldsymbol{x}}. \tag{3.60}$$

Then,

$$\frac{dL}{d\boldsymbol{x}} = \frac{df}{d\boldsymbol{x}} + \lambda^T \left(\frac{d(\boldsymbol{A}(\boldsymbol{x})\boldsymbol{u} - \boldsymbol{B}(\boldsymbol{x}))}{d\boldsymbol{x}} \right), \tag{3.61}$$

$$\frac{dL}{d\boldsymbol{x}} = \frac{\partial f(\boldsymbol{u}, \boldsymbol{x})}{\partial \boldsymbol{x}} + z^T \frac{d\boldsymbol{u}}{d\boldsymbol{x}} + \lambda^T \left(\frac{d(\boldsymbol{A}(\boldsymbol{x})\boldsymbol{u} - \boldsymbol{B}(\boldsymbol{x}))}{d\boldsymbol{x}} \right), \tag{3.62}$$

this calculation is done to each constraint g_j. Applying the product rule we have:

$$\frac{dL}{d\boldsymbol{x}} = \frac{\partial f(\boldsymbol{u}, \boldsymbol{x})}{\partial \boldsymbol{x}} + z^T \frac{d\boldsymbol{u}}{d\boldsymbol{x}} + \lambda^T \left(\frac{d\boldsymbol{A}}{d\boldsymbol{x}}\boldsymbol{u} + \boldsymbol{A}\frac{d\boldsymbol{u}}{d\boldsymbol{x}} - \frac{d\boldsymbol{B}(\boldsymbol{x})}{d\boldsymbol{x}} \right). \tag{3.63}$$

Joining the terms with $d\boldsymbol{u}/d\boldsymbol{x}$ we have:

$$\frac{dL}{d\boldsymbol{x}} = \frac{\partial f(\boldsymbol{u}, \boldsymbol{x})}{\partial \boldsymbol{x}} + (z^T + \lambda^T \boldsymbol{A})\frac{d\boldsymbol{u}}{d\boldsymbol{x}} + \lambda^T \left(\frac{d\boldsymbol{A}}{d\boldsymbol{x}}\boldsymbol{u} - \frac{d\boldsymbol{B}(\boldsymbol{x})}{d\boldsymbol{x}} \right). \tag{3.64}$$

The adjoint variable λ is chosen such that the term that multiplies $d\boldsymbol{u}/d\boldsymbol{x}$ is null and thus it is not necessary to solve the system of equations solved in equation 3.57. For this, the following system must be satisfied:

$$z^T + \lambda^T \boldsymbol{A}(\boldsymbol{x}) = 0 \Rightarrow \lambda^T = -z^T \boldsymbol{A}^{-1}(\boldsymbol{x}). \tag{3.65}$$

Substituting this condition in equation 3.64, we have:

$$\frac{dL}{d\boldsymbol{x}} = \frac{\partial f(\boldsymbol{u}, \boldsymbol{x})}{\partial \boldsymbol{x}} - z^T \boldsymbol{A}^{-1}(x) \left(\frac{d\boldsymbol{A}(\boldsymbol{x})}{d\boldsymbol{x}}\boldsymbol{u} - \frac{d\boldsymbol{B}(\boldsymbol{x})}{d\boldsymbol{x}} \right). \tag{3.66}$$

The Direct and the Adjoint Methods arrive at the same result (see equation 3.58), however, computationally, by different ways. As noted, the direct method is more expensive when the number of design variables is greater than the number of constraints and the adjunct method, in turn, is more expensive when the number of constraints is greater

than the number of design variables [66].

3.4.3.3 Semi-Analytical Method

In the semi-analytical method, the first steps of the analytical method are followed until arriving at equation 3.58 or equation 3.66. In the semi-analytical method, the first steps of the analytical method are followed until arriving at equation 3.58 or equation 3.66. The Semi-Analytical method, however, proposes that the derivatives of the matrices $\boldsymbol{A}(\boldsymbol{x})$ and/or $\boldsymbol{B}(\boldsymbol{x})$ be computed using the finite difference method, that is:

$$\frac{d\boldsymbol{A}(\boldsymbol{x})}{d\boldsymbol{x}} \approx \frac{\boldsymbol{A}(\boldsymbol{x}+\boldsymbol{\Delta x})-\boldsymbol{A}(\boldsymbol{x})}{\Delta \boldsymbol{x}}, \tag{3.67}$$

where $\boldsymbol{\Delta x}$ is a sufficiently small variation in the design variables.

As in the FDM, the approximation to the matrix $\boldsymbol{A}$ must also be done $\boldsymbol{n}$ times, where $\boldsymbol{n}$ is the number of elements of the vector $\boldsymbol{x}$. This can make this method expensive owing to the need to compute the matrix $\boldsymbol{A}$ taking into account the increment $\boldsymbol{\Delta x}$ in each element of the vector. However, this method can be advantageous in cases where $\boldsymbol{A}$ does not explicitly depend on $\boldsymbol{x}$, or when it is very difficult to find an analytic function for the derivative.

3.4.4 Material Model

Evaluating the analytic derivative of the matrix $\boldsymbol{A}$ or $\boldsymbol{B}$ as a function of the design variable $\boldsymbol{x}$ can be challenging for problems where there is no explicit function. For optimization problems, some tricks are used to get around this difficulty. For the special case of the structural problem ($\boldsymbol{Ku} = \boldsymbol{F}$), the matrices $\boldsymbol{A}$ and $\boldsymbol{B}$ are stiffness matrix $\boldsymbol{K}$ and force vector $\boldsymbol{F}$, respectively. A widespread method is the interpolation of the densities $\boldsymbol{x_i}$ through a penalty function.

The SIMP material method (not to be confused with the homonymous optimization method) proposed by [23] interpolates the structural stiffness by:

$$\boldsymbol{K}(\boldsymbol{x_i}) = \mathbf{A} \rightarrow \boldsymbol{x_i}^p \boldsymbol{K_i} \tag{3.68}$$

in which $\boldsymbol{K}$ is the global stiffness matrix, $\boldsymbol{K_i}$ is the element stiffness matrix, and $\boldsymbol{p}$ is a positive penalty.

The derivative of the matrix $\boldsymbol{K}$ as a function of the design variable $\boldsymbol{x_i}$ is given by

$$\frac{d\boldsymbol{K}}{d\boldsymbol{x_i}} = p{\boldsymbol{x_i}}^{p-1}\boldsymbol{K_i}. \tag{3.69}$$

This result can be substituted in Eqs.(3.58) and (3.66) to obtain a complete expression of the analytical methods. Note that, in the above equations, $dF/dx = 0$ $(= dB/dx)$, since the applied force does not depend on the density of the element. Then the sensitivity is:

$$f' = -p{\boldsymbol{x_i}}^{p-1}\boldsymbol{u_n}{\boldsymbol{K_i}}^{-1}\boldsymbol{u_n}. \tag{3.70}$$

where $\boldsymbol{u_n}$ is the displacement of each element.

3.4.5 Topology Optimization

The two main optimization problems in the mechanic industry are the minimization of mechanical stress and the maximization of stiffness. Topology optimization for stress minimization, however, is still an open problem in engineering. The complexity of this problem is explained by the fact that mechanical stress is a local constraint and we have infinite points in the domain where this constraint must be applied, in addition, the removal of elements can cause stress concentration problems, which makes the problem even more complex. This work, however, focuses on compliance minimization.

The most common approach to TO is to use the pseudo-density ρ (hereinafter called density) as the design variable that are assigned for each element in a finite element mesh discretizing the design domain. The stiffness matrix of the structure continuously depends on this variable.

The first approach works with continuous variables and apply a penalty factor to try leading the solution to near black-and-white results. The binary TO methods, on the other hand, keep the original $\rho = \{0\}$ or $\{1\}$ binary variables. The design variable points out where there should or should not be material.

In the SIMP method a "material model" is used to interpolate the problem physics linking it to the continuous design variables. The results using continuous variables are characterized by presenting regions in gray scale, representing the continuous values of the design variable (see figure 15). However, in practice one usually wants a black-and-white design in the macroscale. At the end of the optimization, it is necessary to penalize the gray scale elements using methods keeping the volume constraint active.

Early, in the development TO methods there were mesh dependency issues and the

Figure 15: SIMP characteristic result with gray scale at boundary.

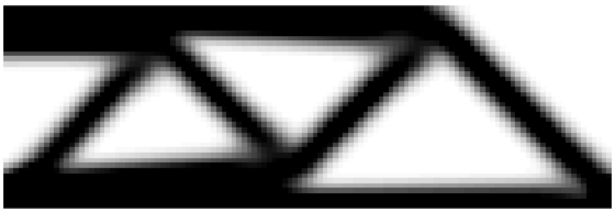

checkerboard pattern appearance in the final solution, or even lack of convergence [67]. *Checkerboard pattern* is a configuration of elements where two neighboring elements are linked by just one node. This configuration presents an artificial stiffness.

This barrier have been overcome by the creation of techniques and filters that leave the solution free of *checkerboard* and mesh-independent [44, 68]. These techniques will be discussed bellow. The BESO method [44] evolved from the idea that less contributing portions of material can be systematically removed (or added) from the structure by evaluating the sensitivity field of the objective function and using a target mass volume. The standard BESO update scheme does not uses mathematical programming and working only on volume restriction. Despite the term "evolutionary" the ESO and BESO methods are gradient-based methods.

The strategy is to order the compliance sensitivities (gradients) in a vector and define as void (or full) the elements that have the lower (or higher) sensitivity values. The choice of the amount of elements to be removed (or added) is controlled by an arbitrary variable that depends on the final volume and is defined by the user heuristically, in other words, it is not based on a automatic and systematic choice. Thus, BESO method ends up being more restricted despite providing a result with explicit structural boundaries [69]. Also, this brings challenges when applying the method to problems without volume constraints [31].

Figure 16: BESO characteristic result with well-defined boundary.

The TOBS is a method that generalizes the binary topology optimization problem

using formal mathematical programming. In this method the original problem is linearized in sub-problems that are solved using the branch-and-bound algorithm. The Branch-and-bound algorithm is a method that solve *Integer Linear Problems*. It consists of a systematic enumeration of all solution candidates, whereby large subsets of unfeasible candidates are discarded using the upper and lower bounds of the optimizable quantity. This allows the method to consider multiple and different constraints, rather than just volume-based one. This method also uses sensitivity filters to avoid both *checkerboard* and mesh-dependency issues. The TOBS method was the first to produce convergent and mesh-independent TO solutions using *Integer Linear Programming* by mean of the branch-and-bound algorithm. Figure 17 shows a characteristic result for minimum compliance problem in the MBB-Beam example. Other TO methods, such as those based on boundary movement will not be considered in this work.

Figure 17: TOBS characteristic result.

3.4.5.1 The TOBS Method

A generic binary optimization problem with inequality constraints is given by

$$\begin{aligned} \underset{x}{\text{Minimize}} \quad & f(x), \\ \text{Subject to} \quad & g_i(x) \leq \overline{g}_i, \ i \in [1, N_g], \\ & x_j = 0 \text{ or } 1, \ j \in [1, N_d], \end{aligned} \tag{3.71}$$

where f is the objective function, g_i is the i^{th} inequality constraint, $\overline{g}_i$ is the associated upper bound and N_g is the number of inequality constraints in the optimization problem.

Since general topology optimization problems are highly nonlinear and non convex, the TOBS method generates and solves approximate integer linear suboptimization problems iteratively. Using the Taylor's series approximation, the objective and constraint functions

can be written as

$$\begin{aligned} f(x) &= f(x^k) + \frac{\partial f(x^k)}{\partial x} \cdot \Delta x^k + O(\left|\left|\Delta x^k\right|\right|_2^2), \\ g_i(x) &= g_i(x^k) + \frac{\partial g_i(x^k)}{\partial x} \cdot \Delta x^k + O(\left|\left|\Delta x^k\right|\right|_2^2), \end{aligned} \tag{3.72}$$

where $(\cdot)^k$ indicates the value of quantity $(\cdot)$ at the iteration k and $O(\left|\left|\Delta x^k\right|\right|_2^2)$ corresponds to superlinear terms. TOBS employs truncated linear approximations of the objective and constraint functions,

$$\begin{aligned} f(x) &\approx f(x^k) + \frac{\partial f(x^k)}{\partial x} \cdot \Delta x^k, \\ g_i(x) &\approx g_i(x^k) + \frac{\partial g_i(x^k)}{\partial x} \cdot \Delta x^k, \end{aligned} \tag{3.73}$$

with the truncation error being $O(\left|\left|\Delta x^k\right|\right|_2^2)$. One can use Δx^k as the vector of change in design variables in order to solve the optimization problem in Equation 3.71. In general, in structural topology optimization, $x_j = 1$ represents a solid element. In this case, one can choose $\Delta x_j \in \{-1, 0\}$ to prescribe that the element j either turns void ($x_j = 0$) or remains solid. The same goes for void elements: one can choose $\Delta x_j \in \{0, 1\}$ prescribing that the element j either turns solid or remains void after solving the integer linear subproblem. The set Δx_j is given to the optimizer as a bound constraint, e.g.,

$$\begin{cases} 0 \leq \Delta x_j^k \leq 1 & \text{if } x_j^k = 0, \\ -1 \leq \Delta x_j^k \leq 0 & \text{if } x_j^k = 1, \end{cases} \tag{3.74}$$

or, in the unified form,

$$\Delta x_j^k \in \{-x_j^k, 1 - x_j^k\}. \tag{3.75}$$

Thus, the optimizer picks optimal Δx_j^k while satisfying the problem constraints and also satisfying integer-only constraints.

In order to maintain the linear approximation (Equation 3.73) valid, the truncation error $O(\left|\left|\Delta x^k\right|\right|_2^2)$ cannot be large. The truncation error is controlled by adding an extra constraint that restricts the number of flips of Δx^k from 1 to 0 and vice-versa. This constraint can be written as

$$\left|\left|\Delta x^k\right|\right|_1 \leq \beta N_d. \tag{3.76}$$

For topology optimization, this means that the number of elements evolving from solid to void and vice-versa in each iteration are restrained to a β fraction of the total number of design variables N_d. Using small values of the control parameter β ensures that the number of flips remains low at each iteration k, thereby keeping the truncation error

small.

Using the sequential linear approximations from Equation 3.73 in the original optimization problem (Equation 3.71) and the extra constraints from Equation 3.75 and Equation 3.76, one can write the approximate integer linear subproblem as

$$\begin{aligned} \underset{\Delta x^k}{\text{Minimize}}\ & \frac{\partial f(x^k)}{\partial x} \cdot \Delta x^k, \\ \text{Subject to}\ & \frac{\partial g_i(x^k)}{\partial x} \cdot \Delta x^k \leq \overline{g}_i - g_i\big(x^k\big) := \Delta g_i^k,\ i \in [1, N_g], \\ & \big|\big|\Delta x^k\big|\big|_1 \leq \beta N_d, \\ & \Delta x_j^k \in \{-x_j^k, 1 - x_j^k\},\ j \in [1, N_d]. \end{aligned} \tag{3.77}$$

Equation 3.77 expresses the sequential optimization subproblems in the standard form solved by TOBS. The term $f(x^k)$ from the linearization (Equation 3.73) is dropped out in Equation 3.77 since scalar addition to the objective function does not alter the optimum design variables. The same is not valid for the constraints. There are some classic equivalences in the optimization context with regard to the objective function and the constraint functions. Minimizing $F(x) + constant$ is the same as minimizing $F(x)$. Imagine a second-degree polynomial function. The value of x that makes $F(x)$ minimal also makes $F(x) + constant$ minimal. It can be shown that this applies to problems with greater degrees and numbers of variables. The constraint function, however, since it works as a boundary that delimits the optimizable domain of the design variables, cannot be changed as this would change that boundary. Note that the term $g_i(x^k)$ is used to compute the right-hand side of the constraint Δg_i^k. The truncation error constraint (Equation 3.76) keeps the topology from undergoing great changes. This might lead to the infeasibility of some of the constraints g_i in the current iteration k when the bound $\Delta g_i^k = \overline{g}_i - g_i\big(x^k\big)$ is used. This can be avoided by modifying the upper bounds of constraints Δg_i^k so that the suboptimization problems yield feasible solutions. This also helps in generating feasible subproblems when the initial solution given to the optimizer is far from being feasible, for instance, starting with a fully solid design domain and having a small volume constraint in the problem. The constraint bounds are modified using

$$\Delta g_i^k = \begin{cases} -\epsilon_i g_i\big(x^k\big) & : \overline{g}_i < (1 - \epsilon_i) g_i\big(x^k\big), \\ \overline{g}_i - g_i\big(x^k\big) & : \overline{g}_i \in [(1 - \epsilon_i) g_i\big(x^k\big), (1 + \epsilon_i) g_i\big(x^k\big)], \\ \epsilon_i g_i\big(x^k\big) & : \overline{g}_i > (1 + \epsilon_i) g_i\big(x^k\big), \end{cases} \tag{3.78}$$

where ϵ_i is the relaxation parameter corresponding to constraint g_i. These parameters

are selected such that the optimization subproblems obtained through linearization yield feasible solutions. The modifications are made such that after the linearized subproblem is solved, the constraint value is expected to remain close enough to the constraint value before solving the subproblem. For instance, when $g_i\left(x^k\right)$ is far from $\overline{g}_i$ and approaches it from above, the upper bound of the linearized constraint g_i is $-\epsilon g_i\left(x^k\right)$. This means that the change of $g_i\left(x^k\right)$ at the iteration k is a fraction ϵ_i of $g_i\left(x^k\right)$ and should enforce a decrease in $g_i\left(x^k\right)$ so that it gradually comes close to $\overline{g}_i$.

The integer optimization subproblems generated using sequential linearization (Equation 3.77) can be solved using Integer Linear Programming (ILP). An ILP problem is the same as a Linear Programming (LP) problem, with additional constraints that the design variables can only have integer solutions. This leads to ILP-based solutions being suboptimal with respect to the LP-based solutions. However, since this topology optimization scheme requires binary $\{0, 1\}$ solutions, integer programming is a reasonable approach. In this work, the ILP problem is solved using the branch-and-bound algorithm implemented in the MATLAB built-in `intlinprog` function, which solves mixed integer linear problems. The branch-and-bound method is an algorithm based on the heap data structure. The ILP is first solved without any integer constraints using some linear optimization techniques.Then branches of LPs are created with additional inequality constraints on the design variables, in order to obtain the final integer solutions. The integer solutions of subproblems $R_{\mathbf{n}}$ are stored for further evaluation of the optimal point (local minimum of the objective function), so that recursive investigations, of the optimization tree (which is the set of all integer solutions found during the search), can be carried out [70, 71]. In other words, the optimizer looks among the previous LP solutions for the one that has the best value for the objective function.

3.4.5.2 Filtering

Numerical filtering is employed in density-based topology optimization approaches to obtain mesh-independent solutions and to avoid the checkerboard pattern problem, as shown in figure 18. This setting has an artificial numerical stiffness. Figure 19 shows an example of the mesh dependency problem.

As shown in figure 19, the optimizer achieves different topologies depending on the discretization. For didactic purposes, in this example, a sensitivity filter was not applied, which leads to mesh dependency results. The filter used and the correct way to apply it is shown below.

Figure 18: Checkerboard Pattern.

Figure 19: Mesh dependency problem: different topologies given by different discretizations.

The filtered sensitivity for an element j is obtained using a weighted average of element sensitivity over the neighborhood of j defined by a filter radius $r_{\min}$.

Figure 20: Numeric filter radius detail shown in a sensitivity plot with colormap.

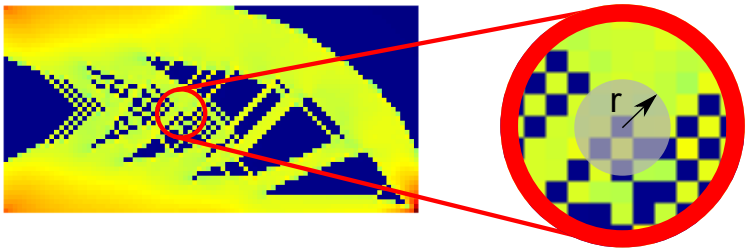

As we can see at figure 20. The larger $r_{\min}$, the smoother the filtered sensitivity.

The filtered sensitivity field $\widetilde{\dfrac{\partial f}{\partial x_j}}$ is given as

$$\widetilde{\frac{\partial f}{\partial x_j}} = \frac{1}{\sum_{m \in N_m} H_{jm}} \sum_{m \in N_m} H_{jm} \frac{\partial f}{\partial x_m}, \tag{3.79}$$

where N_m is the set of elements m for which the center-to-center distance $\texttt{dist}(x_j, x_m)$ from element j is smaller than the filter radius $r_{\min}$, and H_{jm} is a weight factor given by

$$H_{jm} = \texttt{max}(0, r_{\min} - \texttt{dist}(x_e, x_m)). \tag{3.80}$$

The weights are defined such that elements closer to element j contribute more to the

filtered sensitivity of j than more distant elements. The filtered sensitivity $\widetilde{\frac{\partial f}{\partial x_j}}$ and $\widetilde{\frac{\partial g}{\partial x_j}}$ are used in place of $\frac{\partial f}{\partial x_j}$ and $\frac{\partial g}{\partial x_j}$ in the linearized optimization problem in Eq. 3.77.

Filtering increases the chances of void elements to return to solid state, especially near highly stressed solid regions. On the other hand, it may lead to inaccurate assessment of the sensitivity in the void regions. One way to mitigate this is to employ time stabilization for the sensitivity field as proposed by [44]. In practice, the filtered sensitivity field is averaged over two consecutive iterations as

$$\widetilde{\frac{\partial f}{\partial x_j}}^{k} \longleftarrow \frac{\widetilde{\frac{\partial f}{\partial x_j}}^{k} + \widetilde{\frac{\partial f}{\partial x_j}}^{k-1}}{2}. \tag{3.81}$$

In this dissertation, all results use TOBS as optimization method and consider compliance minimization subject to volume, equilibrium and soil-structure interaction constraints. The structural optimizable domain is discretized using finite element method and the soil is modeled using indirect boundary element method in a static analysis.

4 METHODOLOGY

4.1 Structural Problem

Consider a plane strain, linear-elastostatic problem with external mechanical loads acting on a two-dimensional structural domain Ω, where σ is the stress field, b are body forces, D is the elasticity tensor, ϵ is the strain field, $(\cdot)_{(k,l)}$ is the symmetric gradient, u is the displacement field, g is the specified displacement field, ξ indicates x and z coordinates, Γ_g is the part of the boundary where displacement boundary conditions are specified, n_j is the normal vector, t_i is the specified traction loading, and Γ_t is the part of the boundary where traction boundary conditions are specified. Table 1 summarizes the formulation of the strong form of this problem.

Table 1: Strong form for linear elastostatics.

$\sigma_{ij,j} + b_i = 0$	Equilibrium equation
$\sigma_{ij} = D_{ijkl}\epsilon_{kl}$	Constitutive equation
$\epsilon_{kl} = u_{(k,l)}$	Infinitesimal strain tensor
$u = g$ for $\xi \in \Gamma_g$	Essential boundary conditions
$\sigma_{ij}n_j = t_i$ for $\xi \in \Gamma_t$	Natural boundary conditions
$u_i : \Omega \to \mathbb{R}$	Solution map

The variational form of this problem can be given as

$$\begin{gathered}\text{Find } u = \{u_i \boldsymbol{e}_i : u = g \text{ for } \xi \in \Gamma_g,\ u \in \mathcal{S}\} \text{ such that} \\ \int_\Omega \delta u_{(i,j)} D_{ijkl} u_{(k,l)}\ d\Omega = \int_\Omega \delta u_i b_i\ d\Omega + \int_{\Gamma_t} \delta u_i t_i\ d\Gamma\end{gathered} \tag{4.1}$$

where δu_i defines the displacement variations, e_i is the unit vector in the $i-$direction $(i = x, z)$, $\mathcal{S}$ is the solution space for displacements, u and g represent the displacement vector and specified displacement vector at a material coordinate, respectively. Using finite element approximation, Eq. (4.1) becomes

$$\begin{gathered}\text{Find } u^h = \{u^h :\ u^h \in \mathcal{S}^h \subset \mathcal{S} \text{ and } u^h = g^h \text{ for } \xi \in \Gamma_g\} \text{ such that} \\ \int_\Omega \delta {u^h}^T {B^s}^T D B^s u^h\ d\Omega = \int_\Omega \delta {u^h}^T {N^s}^T b\ d\Omega + \int_{\Gamma_t} \delta {u^h}^T {N^s}^T N^s t^h\ d\Omega\end{gathered} \tag{4.2}$$

in which the superscript $(\cdot)^h$ indicates that the quantity $(\cdot)$ is discretized, h indicates the element size, u^h is the vector of nodal displacements, $\mathcal{S}^h$ is the finite element approxima-

tion space, and N^s and B^s are the matrices corresponding to shape functions and their gradients, respectively.

We use Voigt notation for the representation of matrices in this work, and drop the superscript h for the sake of simplicity. Equation (4.2) can be written in the following matrix form

$$Ku = F \tag{4.3}$$

in which K is the stiffness matrix (corresponding to the left-hand side of Eq. (4.2)), F is the f equivalent nodal forces, (corresponding to the right-hand side of Eq. (4.2)). The stiffness matrix and load vectors are obtained by assembling element-wise stiffness matrices (K_e) and element-wise load vectors (F), which are given by

$$\begin{aligned} K_j &= \int_{\Omega_j} B^{sT} D_j B^s \; d\Omega \\ F_j &= \int_{\Omega_j} N^{sT} b \; d\Omega + \int_{\Gamma_t \cap \Gamma_j} N^{sT} N^s t \; d\Omega \end{aligned} \tag{4.4}$$

where Ω_j is the subdomain corresponding to structure finite element j, and Γ_j is the associated finite element boundary. The elasticity tensor for each finite element is modeled using a penalization method like SIMP, such that

$$D_j = x_j^p \overline{D} \tag{4.5}$$

in which $\overline{D}$ is the elasticity tensor for a fully solid finite element, x_j is the design variable to be optimized within optimization context, and $p = 3$ is the penalization factor. In this work, we use $x_j = 1$ and $x_j = 0.001$ to represent solid and void material, respectively. The value $x_j = 0.001$ is used instead of $x_j = 0$ in order to avoid problems with singularities in the finite element matrix.

4.2 Soil-Structure Coupling

Figure 21 illustrates the coupling considered in this formulation. A surface structure is modeled by finite elements and the soil is modeled with the IBEM. This section describes the coupling between the two methods at the interface – the surface of the soil.

In this formulation, the soil is modeled as a homogeneous, two-dimensional, unbounded half-space. The contact interface between the superstructure and the soil is discretized by a number of elements in which displacements and tractions are considered to be uniformly distributed. The superstructure is modeled with linear-elastic, four-noded

Figure 21: Model of soil-structure interaction through an IBEM-FEM coupling scheme.

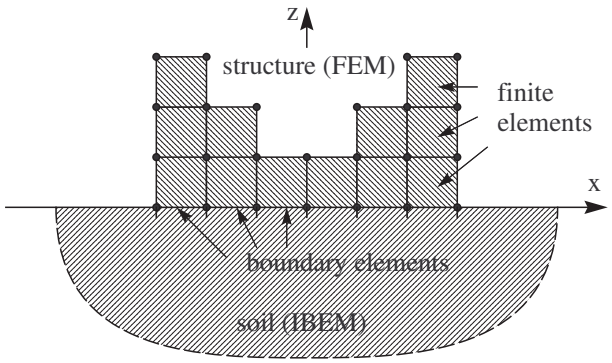

quadrilateral finite elements, with two degree-of-freedom per node (displacements in the $x-$ and $z-$directions). Concentrated or distributed forces can be applied anywhere in the structure in terms of nodal equivalents. The interface is discretized such that there is one boundary element of soil corresponding to each finite element of the structure at the interface. A condition of perfect bonding (no slip) between soil and structure is assumed; perfect continuity condition is imposed at the interface.

4.2.1 Equilibrium at the interface

In this coupling formulation, the influence of the presence of the soil is incorporated in the response of the structure through a set of equivalent nodal contact forces f_s, such that:

$$Ku = F - f_s, \tag{4.6}$$

in which K is the same stiffness matrix of the structure from Eq. (4.3).

The distribution of contact tractions at the interface is unknown. These are approximated by a series of piece-wise constant approximations called fictitious stresses q_i, $(i = x, z)$ (figure 22). Notice that, since the boundary and finite elements have different orders of approximation, the number of nodes in the IBEM discretization is incompatible with those of the FEM discretization.

The distribution of fictitious contact stresses q_i in terms of nodal equivalents f_{si} must account for this difference (figure 23). This transformation is obtained through

$$f_s = Aq, \tag{4.7}$$

Figure 22: Piece-wise constant approximations for contact tractions.

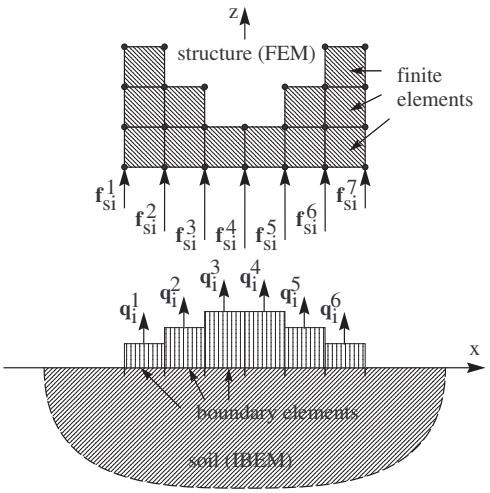

in which

$$f_s = \left\{ f_{sx}^1 \quad f_{sz}^1 \quad f_{sx}^2 \quad f_{sz}^2 \quad \cdots \quad f_{sx}^{n_n} \quad f_{sz}^{n_n} \right\}^T_{2n_n \times 1} \tag{4.8}$$

and

$$q = \left\{ q_x^1 \quad q_z^1 \quad q_x^2 \quad q_z^2 \quad \cdots \quad q_x^{n_s} \quad q_z^{n_s} \right\}^T_{2n_s \times 1} \tag{4.9}$$

in which n_n and n_s are the number of nodes in the FE and BE meshes, respectively, and

$$A = \frac{1}{2} \begin{bmatrix} l_e^1 & 0 & & & & & \\ 0 & l_e^1 & & & & & \\ l_e^1 & 0 & l_e^2 & 0 & & & \\ 0 & l_e^1 & 0 & l_e^2 & & & \\ & & l_e^2 & 0 & & & \\ & & 0 & l_e^2 & & & \\ & & & & \ddots & & \\ & & & & & l_e^N & 0 \\ & & & & & 0 & l_e^N \\ & & & & & l_e^N & 0 \\ & & & & & 0 & l_e^N \end{bmatrix}_{2n_s \times 2n_n}$$

is the transformation matrix, in which l_e^i is the length of finite element i ($i = 1, N$), where $N = 2n_n - 1$ is the total number of finite elements in the interface.

The equilibrium equation for the nodes of the structure at the interface, with the incorporation of the presence of the soil is

$$Ku + Aq = F. \tag{4.10}$$

Figure 23: Coupling between boundary and finite elements.

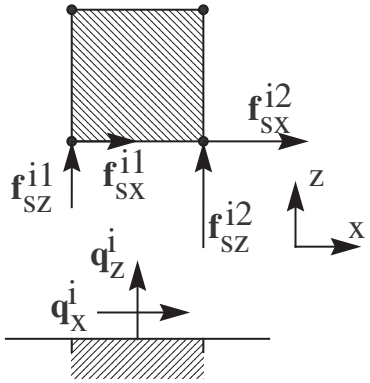

4.2.2 Kinematic compatibility

The displacement w_{si} $(i = x, z)$ of each of the elements of soil in the i-direction due to the contact tractions q_i is given by

$$w_s = Uq, \tag{4.11}$$

in which $w_s = \left\{ w^1_{sx} \quad w^1_{sz} \quad w^2_{sx} \quad w^2_{sz} \quad \cdots \quad w^{n_s}_{sx} \quad w^{n_s}_{sz} \right\}^T_{2n_s \times 1}$ and

$$U = \begin{bmatrix} u^{1,1}_{xx} & u^{1,1}_{xz} & u^{1,2}_{xx} & u^{1,2}_{xz} & \cdots & u^{1,N_b}_{xx} & u^{1,N_b}_{xz} \\ u^{1,1}_{zx} & u^{1,1}_{zz} & u^{1,2}_{zx} & u^{1,2}_{zz} & \cdots & u^{1,N_b}_{zx} & u^{1,N_b}_{zz} \\ u^{2,1}_{xx} & u^{2,1}_{xz} & u^{2,2}_{xx} & u^{2,2}_{xz} & & u^{2,N_b}_{xx} & u^{2,N_b}_{xz} \\ u^{2,1}_{zx} & u^{2,1}_{zz} & u^{2,2}_{zx} & u^{2,2}_{zz} & & u^{2,N_b}_{zx} & u^{2,N_b}_{zz} \\ \vdots & & & & \ddots & & \\ u^{N_s,1}_{xx} & u^{N_s,1}_{xz} & u^{N_s,2}_{xx} & u^{N_s,2}_{xz} & & u^{N_s,N_s}_{xx} & u^{N_s,N_s}_{xz} \\ u^{N_s,1}_{zx} & u^{N_s,1}_{zz} & u^{N_s,2}_{zx} & u^{N_s,2}_{zz} & & u^{N_s,N_s}_{zx} & u^{N_s,N_s}_{zz} \end{bmatrix}_{2N_s \times 2N_s} \tag{4.12}$$

is the influence matrix of the soil, in which $u^{i,j}_{r,s}$ is the displacement of element i in the r-direction due to a *unit* load applied at element j in the s-direction, and $N_s = n_s$ is the number of soil elements. These displacement-field solutions for half-spaces under uniformly distributed loads are called influence functions. Influence functions for this case of surface loads can be found in [19].

In order to impose the continuity condition between the soil and the structure, that the displacement of each soil element equals that of its corresponding structure element, it is necessary to write w_s in terms of nodal equivalents as well. This can be obtained by

$$w_s = Du, \tag{4.13}$$

in which

$$D = \frac{1}{2}\begin{bmatrix} 1 & 0 & 1 & 0 & & & & & \\ 0 & 1 & 0 & 1 & & & & & \\ & 1 & 0 & 1 & 0 & & & & \\ & 0 & 1 & 0 & 1 & & & & \\ & & & & & \ddots & & & \\ & & & & & & 1 & 0 & 1 & 0 \\ & & & & & & 0 & 1 & 0 & 1 \end{bmatrix}_{2n_n \times 2n_s}$$

is the transformation matrix. The continuity condition then yields

$$Du - Uq = 0. \tag{4.14}$$

4.2.3 Equilibrium equation

The final equilibrium equation for the nodes at the interface results from Eqs. 4.10 and 4.14:

$$\begin{bmatrix} K & A \\ D & -U \end{bmatrix} \begin{Bmatrix} u \\ q \end{Bmatrix} = \begin{Bmatrix} F \\ 0 \end{Bmatrix}. \tag{4.15}$$

Notice that this equation involves only the degrees of freedom of the structure that are at the interface. These terms need to be assembled back into the full equilibrium equation of the structure in the appropriate places.

4.2.4 Void regions in the soil

In this work, we include an analysis of the influence of voids in the soil in the optimization procedure. This is important because voids and inclusions alter the flexibility of the soil as well, and in a different way than the constitutive properties of the soil. An illustration of the case considered in this work is shown in figure 24. Two separate points of the structure are in contact with the soil. In an intermediate surface over the void, finite elements of the structure are not coupled with soil elements. The void is modeled by discretizing its contour within the soil with boundary elements, and imposing zero-traction condition throughout the contour. A fundamental difference from the surface structure case is that, in order to impose traction boundary conditions at points within

the soil, stress influence functions must be available as well, and these are significantly more difficult to derive and evaluate numerically than their displacement counterparts.

Figure 24: Illustration of the soil void problem considered in this work.

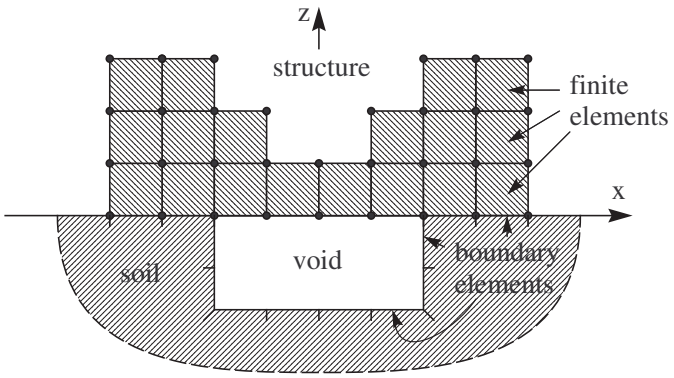

The equilibrium equation of the soil-structure-void problem can be derived in a similar way of Equation 4.15, and results in

$$\begin{bmatrix} K & A \\ D & -C \end{bmatrix} \begin{Bmatrix} u \\ l \end{Bmatrix} = \begin{Bmatrix} F \\ 0 \end{Bmatrix}, \tag{4.16}$$

in which $C = U^{-1}$, and l is the unknown vector of loads exchanged at the structure-soil interface, such that

$$q = -{T_{vv}}^{-1} T_{vp} l, \tag{4.17}$$

for the case in which zero-traction is imposed throughout the contour of the void. T_{vv} and T_{vp} in Equation 4.17 are traction counterparts to the displacement influence matrix U in Equation 4.12. The terms $t^{i,j}_{r,s,m}$ of T_{vv} and T_{vp} are tractions on element i of the void ($m = v$) or of the structure-soil interface ($m = l$) in the r-direction due to a *unit* load applied at element j in the s-direction of an element of m. Traction influence functions are obtained from stress influence functions upon considering the normal vector to the surface in which they are computed, such that $t^{i,j}_{r,s,m} = \sigma^{ik,j}_{r,s,m} n_k$. The normal vector points away from the material portion of the domain, such that in the case of the void $n_k = \{0, 1\}^T$ at the bottom surface of the void, and $n_k = \{1, 0\}^T$ and $n_k = \{-1, 0\}^T$ at its left and right walls, respectively (Figure 24). Differently than the displacement influence functions for surface loads involved in Equation 4.12, stress influence functions for buried loads are not available in the literature. Professor Josué Labaki and Prof. Pérsio Barros both from University of Campinas SP have derived these influence functions for this work, in a academic partnership;

4.3 Topology Optimization Framework

4.3.1 Sensitivity Analysis

The compliance sensitivity with respect to the design variable x_j can be derived using the adjoint method [22]. First, an extended function is written:

$$L = F^T u + \lambda_1^T (Ku + Aq - F) + \lambda_2^T (Du - Uq), \tag{4.18}$$

where λ_1 and λ_2 are arbitrary constants. Deriving L is equivalent to deriving $C(x)$ where both constraints $Ku + Aq = F$ and $Du = Uq$ are satisfied. Notice that the first term from right side is the same expression of compliance. The second and third terms come from equilibrium equation 4.15. The derivative of L can be expressed as

$$\frac{\partial L}{\partial x_j} = F^T \frac{\partial u}{\partial x_j} + \lambda_1^T \left(\frac{\partial K}{\partial x_j} u + K \frac{\partial u}{\partial x_j} + A \frac{\partial q}{\partial x_j} \right) + \lambda_2^T \left(D \frac{\partial u}{\partial x_j} - U \frac{\partial q}{\partial x_j} \right). \tag{4.19}$$

The derivative of F, A, D, and U in this case are 0 since the load and such matrices does not depend on the element density x_j.

The derivative of Equation 4.14 with respect to density is given by

$$D \frac{\partial u}{\partial x_j} = U \frac{\partial q}{\partial x_j} \Rightarrow \frac{\partial q}{\partial x_j} = U^{-1} D \frac{\partial u}{\partial x_j}. \tag{4.20}$$

Substituting the above relation into Equation 4.19, the last term is canceled and the remainder is

$$\frac{\partial L}{\partial x_j} = F^T \frac{\partial u}{\partial x_j} + \lambda_1^T \left(\frac{\partial K}{\partial x_j} u + K \frac{\partial u}{\partial x_j} + A U^{-1} D \frac{\partial u}{\partial x_j} \right). \tag{4.21}$$

The derivatives of the state variables $\dfrac{\partial u}{\partial x_j}$ in Equation 4.21 are usually computationally expensive to evaluate. One can choose a λ_1 such that the terms depending on $\dfrac{\partial u}{\partial x_j}$ are zero,

$$F^T + \lambda_1^T (K + A U^{-1} D) = 0, \tag{4.22}$$

which makes λ_1 assume the following value

$$\lambda_1^T = -F^T (K + A U^{-1} D)^{-1}. \tag{4.23}$$

Using the continuity equation, Equation 4.14, into equilibrium, Equation 4.10, one has

$$Ku + A(U^{-1} D u) = F. \tag{4.24}$$

from which comes

$$u = (K + AU^{-1}D)^{-1}F. \tag{4.25}$$

Comparing Equation 4.23 and Equation 4.25, we can conclude that $\lambda_1^T = -u$. This substitution is possible because the structural compliance function is self-adjoint. For more complex problems, e.g., stress analysis, the solution of a system of equations maybe required to obtain λ_1. Choosing $\lambda_1^T = -u$ and knowing that the terms depending on $\frac{\partial u}{\partial x_j}$ are now canceled out, Eq. 4.21 can be rewritten as

$$\frac{\partial L}{\partial x_j} = \lambda_1^T \frac{\partial K}{\partial x_j} u, \tag{4.26}$$

$$\frac{\partial L}{\partial x_j} = -F^T (K + AU^{-1}D)^{-1} \frac{\partial K}{\partial x_j} u, \tag{4.27}$$

and, finally,

$$\frac{\partial C(x)}{\partial x_j} = \frac{\partial L}{\partial x_j} = -u^T \frac{\partial K}{\partial x_j} u. \tag{4.28}$$

In order to compute the term $\frac{\partial K}{\partial x_j}$ in Equation 4.28 analytically, we interpolate the structural stiffness as

$$K = \sum_{j=1}^{N_d} E(x_j) k_0, \tag{4.29}$$

where k_0 is the element stiffness matrix of a solid element and $E(x_j)$ is an interpolation function of the Young's Modulus. This function can be expressed via the modified SIMP approach [72] as

$$E(x_j) = E_{\min} + x_j^p (E_0 - E_{\min}), \tag{4.30}$$

where E_0 is the stiffness of the solid material, $E_{\min}$ is a very small stiffness assigned to void regions in order to prevent singularities in the global stiffness matrix, and p is a positive penalization factor. The expression in Equation 4.30 can also be called material model. Deriving Equation 4.29 with respect to x_j and substituting its value in Equation 4.28, the final expression for the compliance sensitivity can be obtained:

$$\frac{\partial C}{\partial x_j} = -\frac{1}{2} p x_j^{p-1} (E_0 - E_{\min}) u_j^T k_0 u_j, \tag{4.31}$$

where u_j is the vector of element displacements.

In view of this model, the compliance function can be rewritten in terms of design variables:

$$C(x) = \sum_{j=1}^{N_d} E(x_j) u_j^T k_0 u_j. \tag{4.32}$$

Although the TOBS method is restricted to integer variables, the material model is employed to aid the derivation of sensitivity. When $x_j = 1$, $E(x_j) = E_0$, and when $x_j = 0$, $E(x_j) = E_{\min}$, thus independent of penalty p. The use of binary variables makes the method naturally avoid intermediate densities that create numerical issues when dealing with more complex physics. We advocate that any sensitivity analysis method can be used to find the required sensitivity by the TOBS method, as long as they are only evaluated at the $\{0, 1\}$ bounds. Corroborating with that, Liang and Cheng [73] presented mathematical proof that discrete sensitivities and SIMP-based sensitivities are equivalent.

The sensitivity of the volume constraint depends on $V(x_j)$. The discrete form of $V(x_j) = \int_\Omega x_j d\Omega$ is given as

$$V_x = \sum_{j=1}^{N_d} x_j V_j, \tag{4.33}$$

where V_j is the volume of the element j. Then, the sensitivity of this term is given in the discrete form as:

$$\frac{dV_x}{dx_j} = V_j. \tag{4.34}$$

4.3.2 Filtering

A numerical filter was employed over the sensitivities as showed in equation 3.79. Also an time stabilization for the sensitivity field was used as described in equation 3.81.

4.4 Formulation of Optimization Problem

The minimum compliance problem subject to a volume constraint is used to illustrate structural topology optimization. The corresponding optimization problem is formulated as follows:

$$\begin{aligned} &\underset{x}{\text{Minimize}}\ C(x) = F^T u, \\ &\text{Subject to}\ \frac{V(x)}{V_0} \leq \overline{V}, \\ &\qquad \begin{bmatrix} K & A \\ D & -U \end{bmatrix} \begin{Bmatrix} u \\ q \end{Bmatrix} = \begin{Bmatrix} F \\ 0 \end{Bmatrix}, \\ &\qquad x_j \in \{0, 1\},\ j \in [1, N_d], \end{aligned} \tag{4.35}$$

where x is the vector of design variables of size N_d, $C(x)$ is the structural compliance function, $V(x)$ is the volume of the structure, V_0 is the volume of the initial fully solid design domain and $\overline{V}$ is the upper bound specified on the structural volume fraction.

4.5 Algorithm

The optimization algorithm of the present method is present in the flowchart of Figure 25. The step-by-step methodology is as follow.

Figure 25: Flowchart of the optimization.

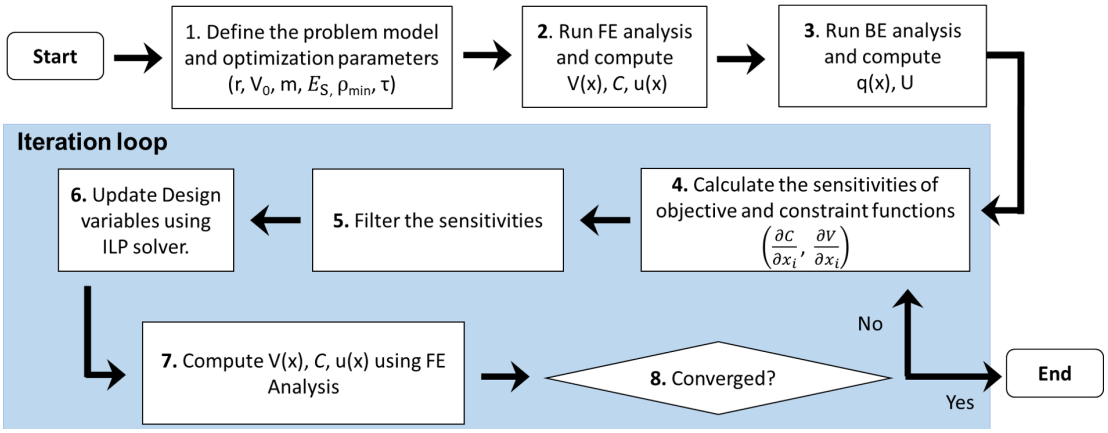

1. Choose the optimization parameters and the soil and structure material properties.
2. Discretize the structure with a finite element mesh.
3. Discretize the soil and compute the soil influence matrix U using Eq. (4.12) and the coupling matrices A and D.
4. Compute the stiffness matrix K, taking into account the design variables expressed in Eq. (4.29), and, obtaining the soil-structure equilibrium equation given in Eq. (4.15) or Eq. (4.16).
5. Compute the compliance sensitivities using Eq. (4.31) and the volume sensitivities using Eq. (4.34).
6. Filter the sensitivities using Eq. (3.79). Incorporate the time stabilization from Eq. (3.81) into the compliance sensitivities.
7. Solve the linearized optimization subproblem from Eq. (3.77) using the ILP solver.
8. Evaluate the convergence of the objective function. If converged, stop. If not converged, repeat from step 4.

5 RESULTS AND DISCUSSIONS

This section considers three soil-structure interaction problems to investigate the influence of soil flexibility in the topology design optimization framework. These problems are a tower, a viaduct, and a bridge, under plane strain case interacting with an isotropic soil of Poisson's ratio $\nu = 0.25$ and Young' modulus E_s. In these analyses, the superstructure is discretized using 4-noded quadrilateral finite elements, of linear-elastic isotropic materials with Poisson's ratio $\nu = 0.25$ and Young's modulus E_0. The minimum value chosen for the Young's modulus for void elements is $E_{min} = 0.001$. Results are presented in terms of the relative structure-to-soil stiffness ratio $m = E_0/E_s$. Increasing values of m correspond to more flexible soils, given a fixed stiffness of the structure. In engineering practice, $m \gg 1$. Results are presented in terms of the normalized compliance $C^* = C_{N_k}/C_1$, in which C_k is the compliance of the structure at the k^{th} iteration ($k = 1, N_k$).

The optimization parameters used throughout this section are shown in Table 2. The radius r of the sensitivity filter was chosen according to the discretization and its value is specified in each case.

Table 2: Optimization parameters used in this section.

Optimization parameters	Value
Density (SIMP) penalization (p)	3
Constraint relaxation parameter (ϵ)	0.01
Truncation error constraint parameter (β)	0.05
Convergence tolerance (τ)	0.001

5.1 The Tower

The present example was proposed to consider a slender structure, in which the region of contact with the soil is small compared to the other dimensions. This example consists of a 6 m tall, 2 m wide tower resting on the soil surface (figure 26). Horizontal and vertical point loads are applied on the center point of the top of the tower. The domain is discretized with 100×300 elements. Compliance optimization is considered, subject to a prescribed 50% volume fraction, with filter radius $r_{\min} = 0.2$ m. These analyses consider $m = \{1, 10, 10^2, 10^3, 10^4 \text{ and } 10^5\}$, and the case of tower over a rigid base is included for comparison.

Figure 26: Elastic tower over elastic soil under (a) horizontal and (b) longitudinal loads.

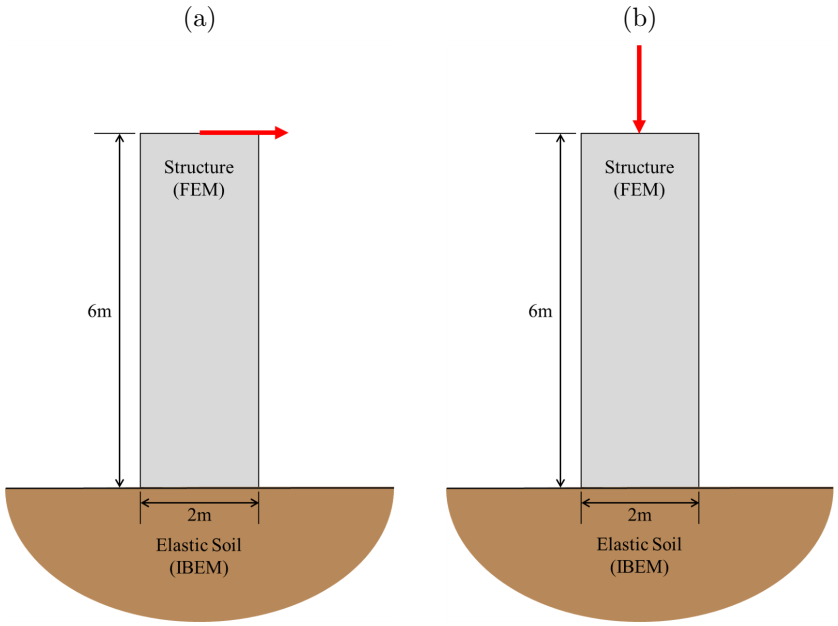

5.1.1 Tower under horizontal load

This section considers the case of the tower under horizontal load. The final optimized topology for different values of soil flexibility is shown in figure 27. Figures 27c and 27d show that the base of the two outer vertical frames of the tower begin to thicken up for $m = 10$, in order to compensate for the effect of the flexibility of the soil in that region. For more flexible soils ($m = 10^2$, 10^3, 10^4 and 10^5), a horizontal bar materializes at the base of the tower, in order to compensate for the increased flexibility of the soil. This bar works as a stiffening link, which prevents the horizontal displacement of the two frames, and helps to reduce the compliance of the structure as a whole. There is also a general tendency for the diagonal braces to be organized more closely to the base of the tower as the soil becomes more flexible. This indicates that the optimization procedure identifies the increased flexibility of the bottom portion of the system and distributes its volume accordingly. Figure 28 shows the compliance and volume fraction history versus iteration steps of the optimization procedure for the case considering $m = 10^4$.

5.1.2 Tower under vertical load

Figure 29 shows the optimized topology obtained for the case of the tower under vertical loading. These results consider $m = \{1,\ 10,\ 10^2$ and $10^3\}$. Figure 29a shows that the optimized topology for the tower over a rigid base is the classical result obtained for a clamped-free bar under plane strain case: two continuous links connect the rigid base

Figure 27: Optimized topologies for the (a) tower over rigid base and for (b) $m = 1$, (c) $m = 10$, (d) $m = 10^2$, (e) $m = 10^3$, (f) $m = 10^4$ and (g) $m = 10^5$.

(a) rigid base, $C^* = 1.4235$ (b) $m = 1$, $C^* = 1.4187$ (c) $m = 10$, $C^* = 1.3896$ (d) $m = 10^2$, $C^* = 1.4068$

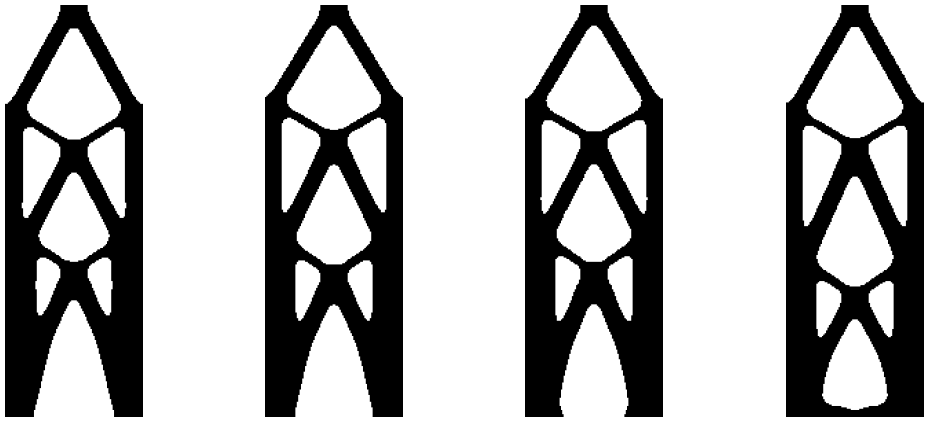

(e) $m = 10^3$, $C^* = 1.4039$ (f) $m = 10^4$, $C^* = 1.4014$ (g) $m = 10^5$, $C^* = 1.2119$

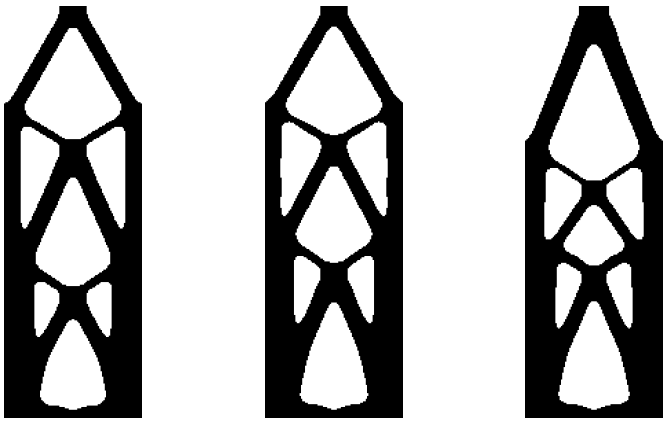

to the loading surface. As the flexibility of the soil increases, the general tendency is that these two links branch off near the soil, and an additional horizontal link begins to materialize, connecting the tip of the branches together and to the soil surface. Figure 30 shows the compliance and volume fraction history during the iterative steps of the optimization procedure for the case in which $m = 10^2$.

A cross-check analysis was also carried out. Consider cases b and e shown in Figs. 29b and 29e, respectively. Let E_s^b and E_s^e be the Young's modulus of the soil in each case, such that $m = E_0^b/E_s^b = 1$ and $m = E_0^e/E_s^e = 10^3$, with $E_0^b = E_0^e$. The optimal topology obtained for the tower in case b was then coupled with the soil from case e, and the compliance and displacement responses were computed for this new coupled system in which the tower and the soil have Young's moduli E_0^b and E_s^e, respectively. Results

Figure 28: Compliance and volume fraction history for the case of tower under horizontal load and $m = 10^4$.

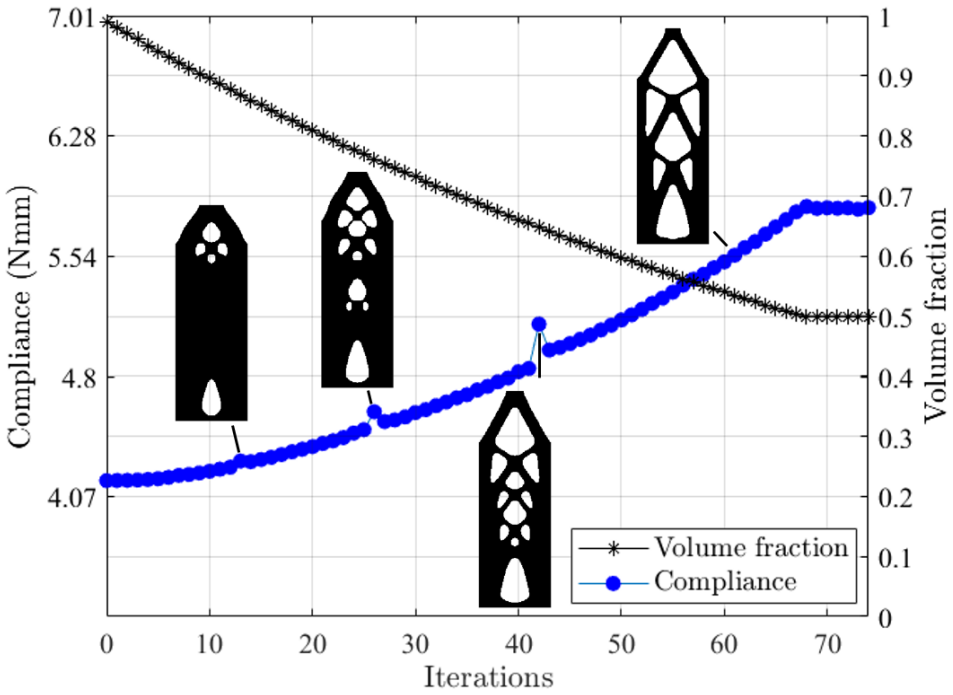

Figure 29: Optimized topology of (a) tower over rigid base, and (b) $m = 1$, (c) $m = 10$, (d) $m = 10^2$, and (d) $m = 10^3$.

(a) Rigid base,	(b) $m = 1$,	(c) $m = 10$,	(d) $m = 10^2$,	(e) $m = 10^3$,
$C^* = 1.4232$	$C^* = 1.4190$	$C^* = 1.4260$	$C^* = 1.4202$	$C^* = 1.4180$

are shown in figure 31. The colormap in this figure shows the total displacement field $(u_x^2 + u_z^2)^{1/2}$ in the body of the tower. Structure is shown with deformation multiplied to a scale of 10. The value of the normalized compliance (C^*) measured for the system is also shown. Figure 31b shows for comparison the results obtained for the tower with E_0^e, that is, the tower that had been optimized for this particular soil case. These results show

Figure 30: Compliance and volume fraction history for the case of tower under vertical load and $m = 10^2$.

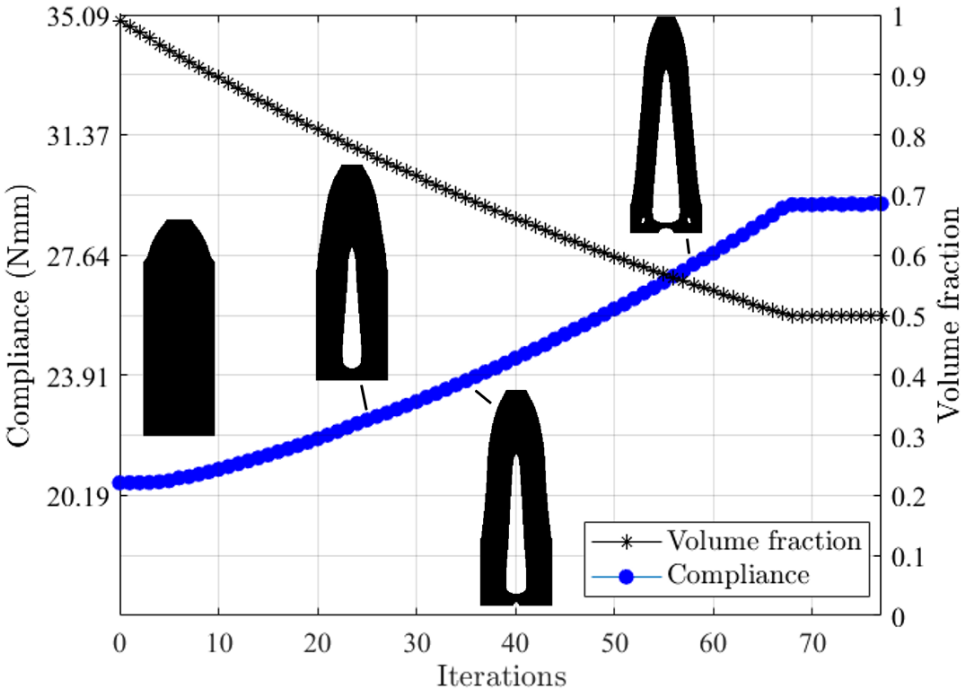

that the topology that had been optimized for soil b performs considerably worse than the design that had been optimized for the soil with which the tower actually interacts. This attests that the optimization procedure considering the elasticity of the soil leads to better designs.

Figure 31: Displacement field and final compliance obtained for the vertically-loaded tower interacting with soil E_s^e, for the optimal topologies obtained for a) E_s^b and b) E_s^e. Displacement fields are multiplied by 10 a large factor in order to improve visualization.

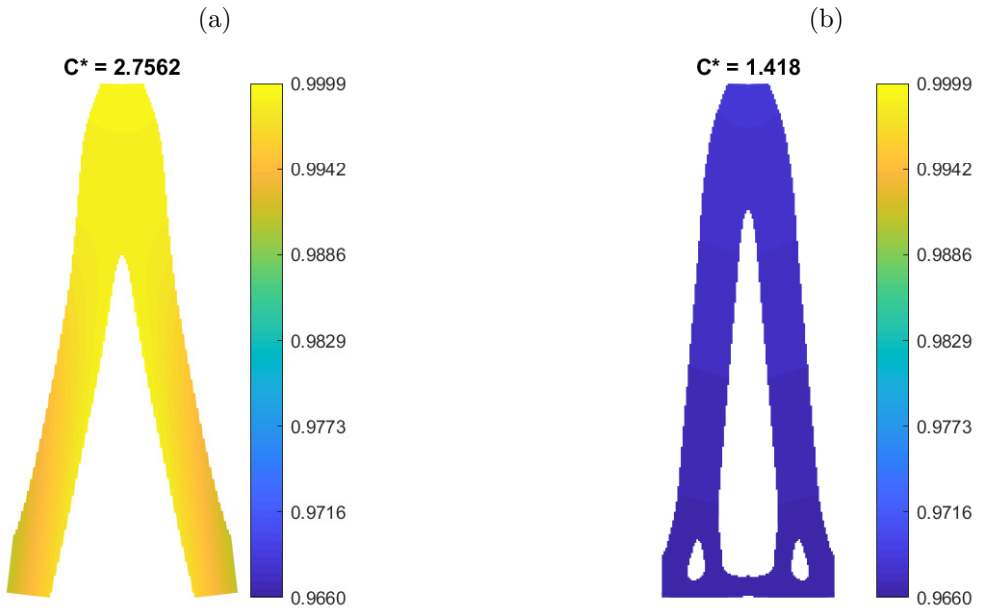

5.2 The Viaduct

This viaduct problem significantly differs from the previous tower problem. In the present problem the structure is connected to the soil in two different, distant points. The presence of the soil corresponds to a flexible connection between these two supports, which must be compensated in some way by the optimization algorithm. Additionally, solid and void passive element regions are incorporated into the viaduct, in order to study the performance of the present method in a variety of situations. The domain of the problem in the $x - z$ plane is given by a 40×20 m rectangle minus a circular cut-out of radius 20.6 m centered at 10 m below the surface of the soil (figure 32). The domain is discretized by 400×200 elements. The structure has two regions with passive elements. The black strip at the top of the viaduct and the white arch in the bottom are modeled with solid and void passive elements, respectively. Solid and void passive elements keep their density 1 and 0, respectively, throughout the optimization procedure. These are defined in order to represent usable traffic space overhead and underneath the viaduct. A uniformly distributed downward vertical load is applied over the top of the viaduct, representing loads that it may undertake on its deck.

This analysis considers the compliance minimization under a prescribed volume fraction of 40%, using a filter of $r_{\min} = 0.3$, such that the filter covers 3 neighboring elements. Figure 33 shows the optimized topologies for $m = \{10,\ 10^2$ and $10^3\}$. The case of the viaduct over a rigid base is included for comparison.

For stiffer soils such as $m = 10$ in figure 33b, the optimized topologies show a structure that arches over the prescribed passive void region, in a very close topology to rigid soil case in figure 33a As the soil becomes more flexible, $m = 10^2$ in figure 33c, center bars appear as a way to constrain horizontal displacements at the base, this had been seen with the tower problem as well. In addition, the main arch changes its configuration to accommodate these center bars. For the case $m = 10^3$ more horizontal bars materialize in the center of the topology over the non-optimizable empty region and the main arch features an upside-down U-shape. Two slender columns appear on outer side of the structure as a way to support the ends of the deck.

5.3 The Bridge

This problem is modeled to represent the case in which a bridge is supported by the shoulders of a canal (figure 34). This analysis is important because inclusions and voids in

Figure 32: Structural domain of the viaduct (a) over a rigid base and (b) on the soil surface.

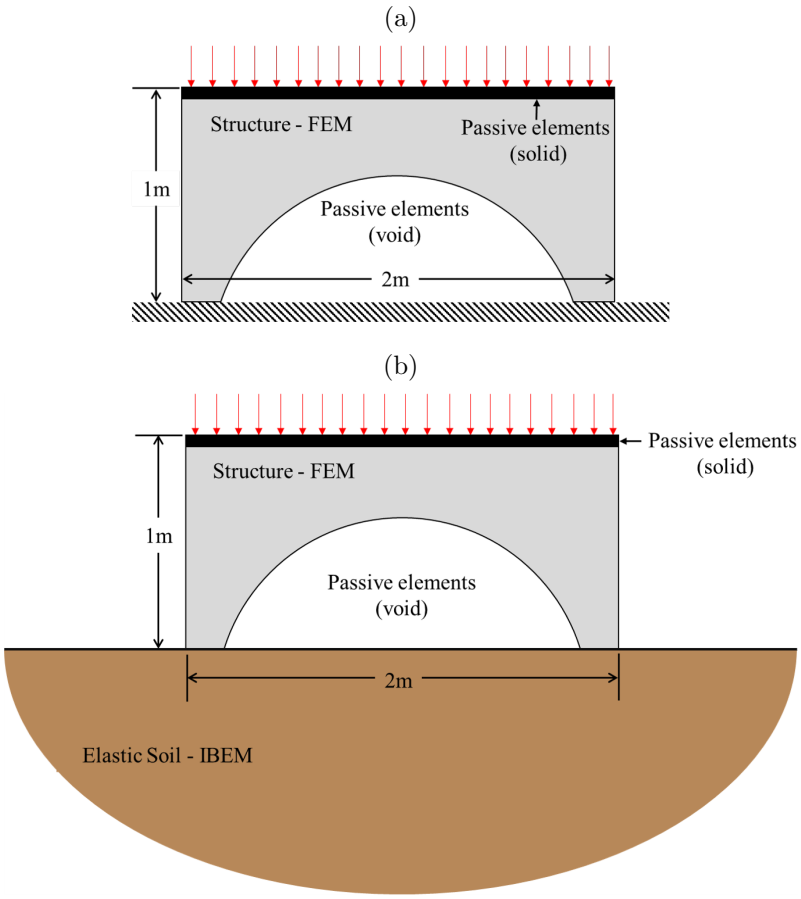

the soil affect its flexibility, even if its constitutive properties are the same. Additionally, the presence of the void in the soil causes different contact points between the bridge and the soil to have different flexibility, and in different directions. It is important to understand how this affects the optimization process.

The canal is modeled by discretizing its contour within the soil with boundary elements, and imposing free traction condition throughout the contour. In order for this to be possible, original influence functions corresponding to buried horizontal and vertical loads had to be derived for this model.

A 1.2 m thick layer of solid passive elements is prescribed on top of the bridge to account for a usable overhead traffic surface, where uniformly distributed, downward vertical loads are applied. The structural domain measuring 40 $\times$ 20 m was discretized using 400×200 finite elements. The soil is a 40 m deep layer over rigid bedrock, containing a 24 m wide canal of depth d. The variable d is introduced here so that canals of different depths can be considered. The bridge-soil interface was discretized with 160 boundary elements, and the bottom and sides of the canal were discretized with 50 and 40 boundary

Figure 33: Optimized topologies for the (a) viaduct over rigid base and (b) $m = 10$, (c) $m = 10^2$, and (d) $m = 10^3$.

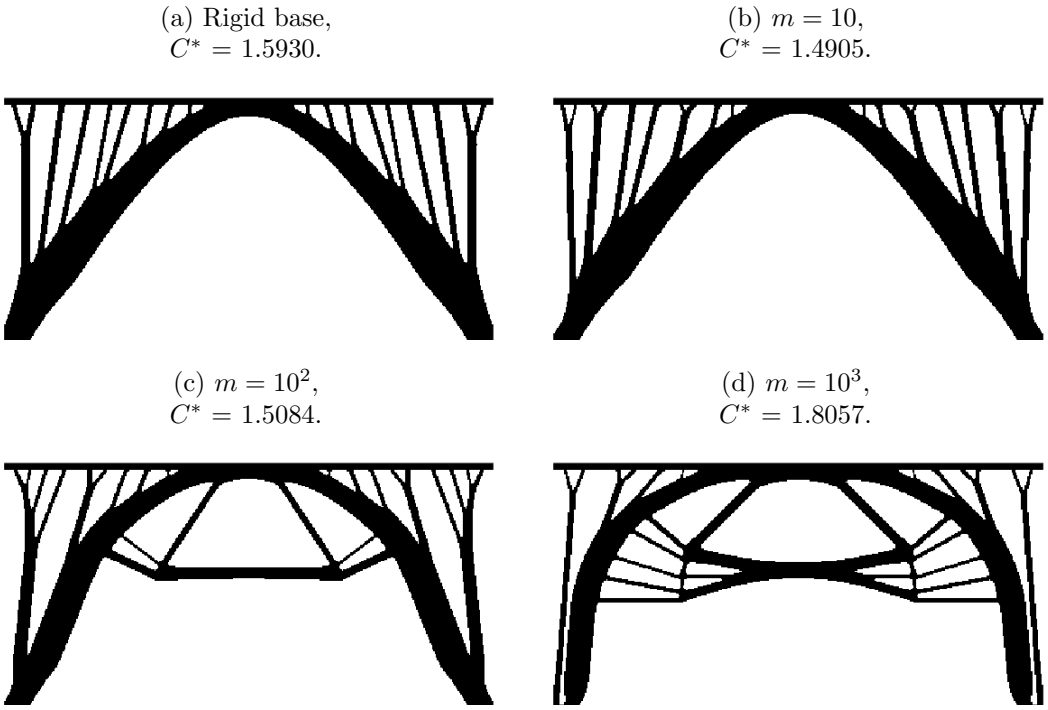

elements, respectively.

Figure 34: Structural domain and boundary conditions of the bridge over a canal.

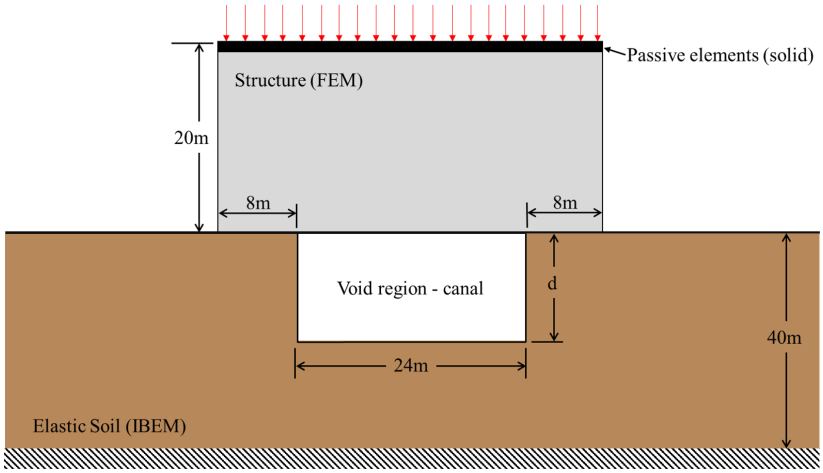

This analysis considers the compliance minimization under a prescribed volume fraction of 40% and filter radius of $r_{\min} = 0.3$ m, which covers 3 neighboring elements. Different bridge-soil stiffness ratios are considered, $m = 1$, $m = 10$, 10^2, 10^3 and 10^4. Figure 35 shows the optimized topology obtained for each value of m using $d = 20$ m. The case of the bridge over rigid supports is included for comparison. These results show that taking into account the flexibility of the soil has a significant impact on the optimized topology. The horizontal bar that had been observed in the previous tower and viaduct

problems is present in the bridge problem even for stiffer soils ($m = 1$, in which the soil is as stiff as the bridge; a theoretical limit that does not even occur in engineering practice). A significant percentage of the material is allocated by the optimization algorithm to the bottom portion of the bridge. For more flexible soils, struts begin to materialize to support the center of the main bridge arch. The thicker strut at the bottom of the bridge is under traction, as show in figure 36a, which indicates that its function is to contain the horizontal displacement of the outer legs of the main arch structure. The inclined struts inside the main arch are under compression, which indicates that their function is to assist with bearing the loads from the deck. It can be pointed out that the present formulation does not include buckling optimization, which is recommended in a future work.

Figure 35: Optimized topologies for the bridge with different values of soil flexibility (a) over rigid soil, (b) $m = 10$, (c) $m = 10^2$, (d) $m = 10^3$ and (e) $m = 10^4$, over a canal of $d = 20$ m.

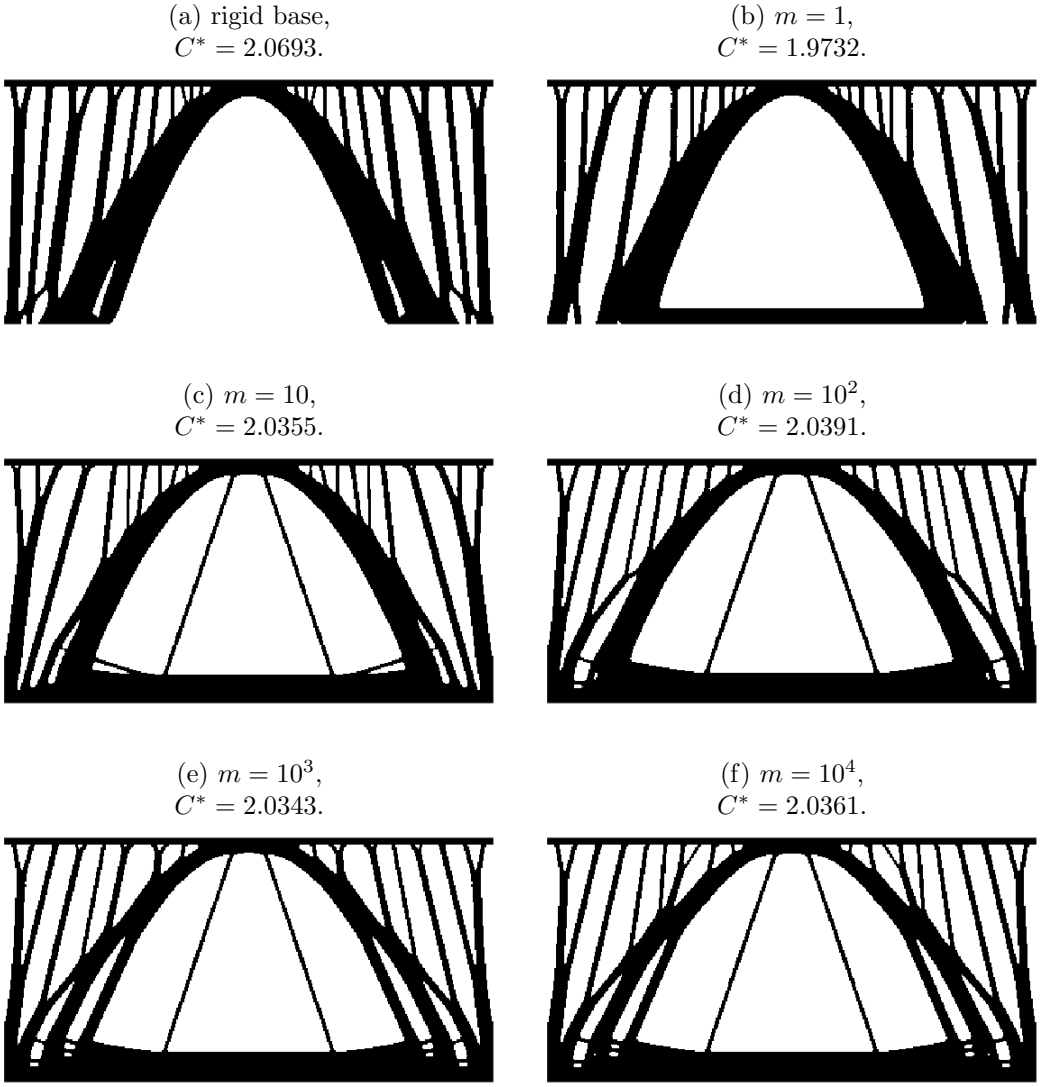

Figure 37 shows the optimized topology of the bridge when different canal depths are

Figure 36: Stress distribution in the bridge designed for $m = 10^3$ over a canal of $d = 20$ m.

(a) Normal stress in x direction, σ_{xx}.

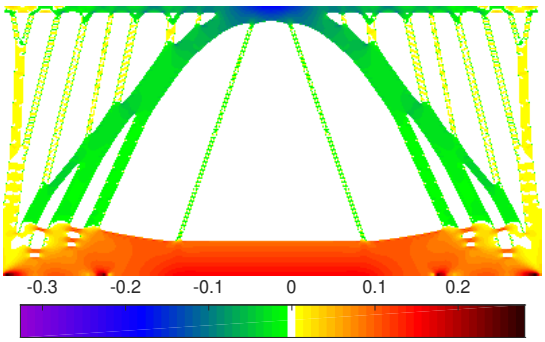

(b) Normal stress in z direction, σ_{zz}.

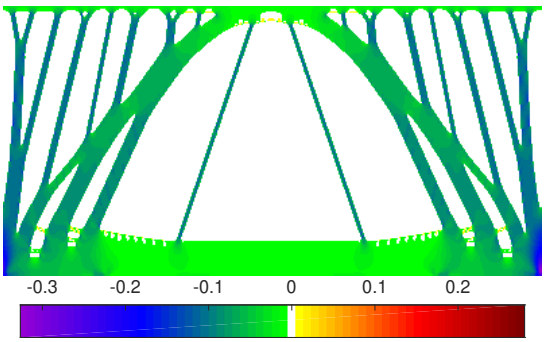

considered. These results consider $d = 10$, 20 and 30 m, for a relative soil flexibility of $m = 10^2$. The case of no canal ($d = 0$), in which the bridge is in contact with the soil throughout its bottom surface, is included for comparison. Table 3 shows quantitative results from this problem. It shows the compliance of the initial and optimized designs, as well as the relative compliance C^*.

Figure 37: Optimized topology for the bridge for three different values of canal depth, using $m = 10^2$.

(a) $d = 0$ (no canal)

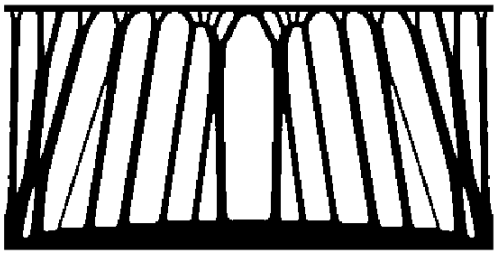

(b) $d = 10$m

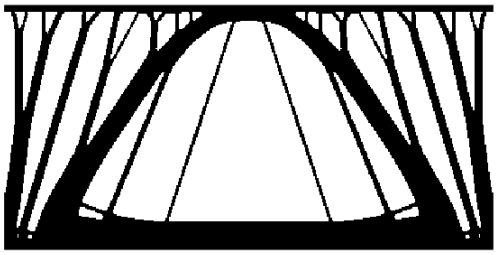

(c) $d = 20$m

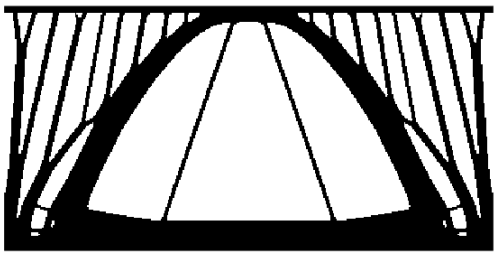

(d) $d = 30$m

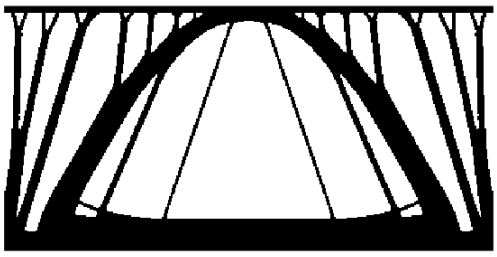

These results support the initial argument that voids in the soil alter its flexibility, regardless of the soil's constitutive properties. The optimized topology of the no-canal case resembles that of a series of bars, with branched-off, interconnected ends to compensate for the soil flexibility. The inclusion of even a shallow canal ($d = 10$ m) causes drastic changes in the optimized topology. In all $d \neq 0$ cases, a significant portion of the material

available is allocated to create a thick horizontal brace connecting the two supports of the bridge. Inclined struts are created with different thicknesses and at different positions depending on the depth of the canal.

A comparison between the $d = 20$ m and the $d = 30$ m cases, however, indicate that after a certain depth, the influence of the depth of the canal in the optimized topology is negligible. This is understandable: although deeper canals continuously affect the flexibility of deeper portions of the soil, their effect on the shoulders of the canal, where the bridge rests, begins to be negligible at some point.

Table 3: Compliance values for the bridge problem with different depths of the canal.

	$C_1\,(Nm)$	$C_{N_k}\,(Nm)$	C^*
$d = 0$ m	0.0032	0.0070	2.1880
$d = 10$ m	0.0059	0.0122	2.0700
$d = 20$ m	0.0065	0.0133	2.0391
$d = 30$ m	0.0068	0.0136	2.0106

6 CONCLUSIONS

This dissertation proposes and investigates the TOBS method applied to problems of soil-structure interaction. For the best of the our knowledge the field of TO considering SSI was still unexplored. It is hoped that the examples proposed in this dissertation will serve as benchmarks for future work on this field. In this work a combination of the FEM and IBEM is proposed for TO problems using the TOBS method. The FEM is used to model the structure and the IBEM is used to model the isotropic elastic soil. The advantages of using the IBEM to model the soil, instead of the FEM, was the capability to model a infinite domain by discretizating only the soil-structure interface. Coupling between soil and structure was successfully obtained by imposing compatibility and equilibrium conditions at their shared interface.

Numerical results showed that the effects of the soil-structure connection are relevant when designing a structure via topology optimization for different ratios of structure-to-soil stiffness and the flexibility of the soil must be taken under consideration in the design of a structure via topology optimization.

Future works include the consideration of material or geometry nonlinearities. Also, the results presented here are only for 2D models and next work include considering 3D models. The application in multiphysics or multiobjective problems, such as the study of the optimization of submerged structures subject to iteration with the seabed and simultaneously subjected to fluid-structure iteration from the sea can be studied in future works. Finally, a series of dynamic analyzes can be performed on these results to take advantage of the BEM features.

REFERENCES

1 PUCKER, T.; GRABE, J. Structural optimization in geotechnical engineering: basics and application. *Acta Geotechnica*, Springer, v. 6, n. 1, p. 41–49, 2011.

2 BENDSOE, M. P.; SIGMUND, O. *Topology optimization: theory, methods, and applications*. [S.l.]: Springer Science & Business Media, 2013.

3 HAMIDI, F.; ASLANI, F. Additive manufacturing of cementitious composites: Materials, methods, potentials, and challenges. *Construction and Building Materials*, v. 218, p. 582–609, 2019. ISSN 0950-0618. Disponível em: ⟨https://www.sciencedirect.com/science/article/pii/S0950061819313194⟩.

4 SIVAPURAM, R.; PICELLI, R. Topology optimization of binary structures using integer linear programming. *Finite Elements in Analysis and Design*, v. 139, p. 49–61, 2018.

5 SELVADURAI, A. P. *Elastic analysis of soil-foundation interaction*. [S.l.]: Elsevier, 2013.

6 DUTTA, S.; ROY, R. A critical review on idealization and modeling for interaction among soil–foundation–structure system. *Computers Structures - COMPUT STRUCT*, v. 80, p. 1579–1594, 08 2002.

7 WINKLER, E. *Die Lehre von der Elasticitaet und Festigkeit: mit besonderer Rücksicht auf ihre Anwendung in der Technik für polytechnische Schulen, Bauakademien, Ingenieue, Maschinenbauer, Architecten, etc.* [S.l.]: Dominicus, 1867. v. 1.

8 TERZAGHI, K. Evalution of conefficients of subgrade reaction. *Geotechnique*, Thomas Telford Ltd, v. 5, n. 4, p. 297–326, 1955.

9 FILONENKO-BORODICH, M. Some approximate theories of elastic foundation. *Uchenyie Zapiski Moskovkogo Gosudarstuennogo Universiteta Mekhanika, Moscow*, v. 46, p. 3–18, 1940.

10 PASTERNAK, P. On a new method of an elastic foundation by means of two foundation constants. *Gosudarstvennoe Izdatelstvo Literaturi po Stroitelstuve i Arkhitekture*, 1954.

11 BOUSSINESQ, J. *Application des potentiels à l'étude de l'équilibre et du mouvement des solides élastiques: principalement au calcul des déformations et des pressions que produisent, dans ces solides, des efforts quelconques exercés sur une petite partie de leur surface ou de leur intérieur: mémoire suivi de notes étendues sur divers points de physique, mathematique et d'analyse*. [S.l.]: Gauthier-Villars, 1885. v. 4.

12 VLASOV, V. Z. Beams, plates and shells on elastic foundation. *Israel Program for Scientific Translation*, 1966.

13 TURNER, M. J. et al. Stiffness and deflection analysis of complex structures. *journal of the Aeronautical Sciences*, v. 23, n. 9, p. 805–823, 1956.

14 WANG, Y.; THAM, L.; CHEUNG, Y. Beams and plates on elastic foundations: a review. *Progress in Structural Engineering and Materials*, Wiley Online Library, v. 7, n. 4, p. 174–182, 2005.

15 GODBOLE, P.; VILADKAR, M.; NOORZAEI, J. Nonlinear soil-structure interaction analysis using coupled finite-infinite elements. *Computers & structures*, Elsevier, v. 36, n. 6, p. 1089–1096, 1990.

16 BARBOSA, J. M. de O.; PARK, J.; KAUSEL, E. Perfectly matched layers in the thin layer method. *Computer Methods in Applied Mechanics and Engineering*, v. 217-220, p. 262–274, 2012. ISSN 0045-7825. Disponível em: ⟨https://www.sciencedirect.com/science/article/pii/S0045782511003859⟩.

17 KOKKINOS, F.; SPYRAKOS, C. Dynamic analysis of flexible strip-foundations in the frequency domain. *Computers & structures*, Elsevier, v. 39, n. 5, p. 473–482, 1991.

18 BARROS, P. L. de A.; LABAKI, J.; MESQUITA, E. IBEM-FEM model of a piled plate within a transversely isotropic half-space. *Engineering Analysis with Boundary Elements*, Elsevier, v. 101, p. 281–296, 2019.

19 POULOS, H. G.; DAVIS, E. H. *Elastic solutions for soil and rock mechanics*. [S.l.]: Wiley New York, 1974. v. 582.

20 CORTEZ, R. et al. On the influence of soil flexibility in structural topology optimization. *Paper Under Review in Computers & Structures*, Elsevier, 2022.

21 MICHELL, A. G. M. The limits of economy of material in frame structures. *Philosophical Magazine*, v. 8, n. 6, p. 589–597, 1904.

22 HAFTKA, R. T.; GÜRDAL, Z. *Elements of Structural Optimization*. 3rd rev. and expanded ed.. ed. [S.l.]: Kluwer Academic Publishers, 1991.

23 BENDSØE, M. P.; SIGMUND, O. *Topology Optimization - Theory, Methods and Applications*. Berlin Heidelberg: Springer Verlag, 2003. XIV+370 p.

24 BENDSØE, M. P.; KIKUCHI, N. Generating optimal topologies in structural design using a homogenization method. *Computer Methods in Applied Mechanics and Engineering*, v. 71, p. 197–224, 1988.

25 ROZVANY, G. I. N.; ZHOU, M.; BIRKER, T. Generalized shape optimization without homogenization. *Structural Optimization*, v. 4, p. 250–254, 1992.

26 SIGMUND, O. A 99 line topology optimization code written in matlab. *Structural and Multidisciplinary Optimization*, v. 21, p. 120–127, 2001.

27 XIE, Y. M.; STEVEN, G. P. A simple evolutionary procedure for structural optimization. *Computer and Structures*, v. 49, p. 885–896, 1993.

28 XIE, Y. M.; HUANG, X. *Evolutionary Topology Optimization of Continuum Structures: Methods and Applications*. 1st. ed. West Sussex: John Wiley & Sons, Ltd, 2010. IX+223 p.

29 SIVAPURAM, R. et al. On the design of multimaterial structural topologies using integer programming. *Computer Methods in Applied Mechanics and Engineering*, v. 384, p. 114000, 2021.

30 ALLAIRE, G.; JOUVE, F.; TOADER, A.-M. Structural optimization using sensitivity analysis and a level-set method. *Journal of Computational Physics*, v. 194, p. 363–393, 2004.

31 DEATON, J. D.; GRANDHI, R. V. A survey of structural and multidisciplinary continuum topology optimization: post 2000. *Structural and Multidisciplinary Optimization*, v. 49, p. 1–38, 2014.

32 ROZVANY, G. I. N. A critical review of established methods of structural topology optimization. *Structural and Multidisciplinary Optimization*, v. 37, p. 217–237, 2009.

33 DIAZ, A. R.; BENDSOE, M. P. Shape optimization of structures for multiple loading situations using a homogenization method. *Structural Optimization*, v. 4, p. 17–22, 1992.

34 DIAZ, A.; KIKUCHI, N. Solutions to shape and topology eigenvalue optimization problems using a homogenization method. *International Journal for Numerical Methods In Engineering*, v. 35, p. 1487–1502, 1992.

35 HAMMER, V. B.; OLHOFF, N. Topology optimization of continuum structures subjected to pressure loading. *Structural and Multidisciplinary Optimization*, v. 19, p. 85–92, 2000.

36 DU, J.; OLHOFF, N. Topological design of vibrating structures with respect to optimum sound pressure characteristics in a surrounding acoustic medium. *Structural and Multidisciplinary Optimization*, v. 42, p. 43–54, 2010.

37 SIGMUND, O. On the design of compliant mechanisms using topology optimization. *Mechanics of Structures and Machines*, v. 25, n. 4, p. 495–526, 1997.

38 SIGMUND, O.; CLAUSEN, P. M. Topology optimization using a mixed formulation: An alternative way to solve pressure load problems. *Computer Methods in Applied Mechanics and Engineering*, v. 196, p. 1874–1889, 2007.

39 WANG, C.; ZHAO, M.; GE, T. Structural topology optimization with design-dependent pressure loads. *Structural and Multidisciplinary Optimization*, v. 53, p. 1005–1018, 2016.

40 LUNDGAARD, C. et al. Revisiting density-based topology optimization for fluid-structure-interaction problems. *Structural and Multidisciplinary Optimization*, online, 2018.

41 LE, C. et al. Stress-based topology optimization for continua. *Structural and Multidisciplinary Optimization*, v. 41, p. 605–620, 2010.

42 DU, J.; OLHOFF, N. Topological design of freely vibrating continuum structures for maximum values of simple and multiple eigenfrequencies and frequency gaps. *Structural and Multidisciplinary Optimization*, v. 34, p. 91–110, 2007.

43 CHEN, Z. et al. A new geometrically nonlinear topology optimization formulation for controlling maximum displacement. *Engineering Optimization*, Taylor & Francis, v. 53, n. 8, p. 1283–1297, 2021.

44 HUANG, X.; XIE, Y. M. Convergent and mesh-independent solutions for the bi-directional evolutionary structural optimization method. *Finite Elements in Analysis and Design*, v. 43, p. 1039–1049, 2007.

45 LIANG, Y.; CHENG, G. Topology optimization via sequential integer programming and canonical relaxation algorithm. *Computer Methods in Applied Mechanics and Engineering*, v. 348, p. 64 – 96, 2019. ISSN 0045-7825.

46 HUANG, X.; XIE, Y. M. Bi-directional evolutionary topology optimization of continuum structures with one or multiple materials. *Computational Mechanics*, v. 43, p. 393–401, 2009.

47 XIE, Y. M.; STEVEN, G. P. Evolutionary structural optimization for dynamic problems. *Computer and Structures*, v. 58, p. 1067–1073, 1996.

48 YANG, X. Y. et al. Bidirectional evolutionary method for stiffness optimization. *AIAA Journal*, v. 37, p. 1483–8, 1999.

49 HUANG, X.; XIE, Y. M. Topology optimization of nonlinear structures under displacement loading. *Engineering Structures*, v. 30, p. 2057–2068, 2008.

50 PICELLI, R.; VICENTE, W. M.; PAVANELLO, R. Bi-directional evolutionary structural optimization for design-dependent fluid pressure loading problems. *Engineering Optimization*, v. 47, n. 10, p. 1324–1342, 2015.

51 PICELLI, R. et al. Evolutionary topology optimization for natural frequency maximization problems considering acoustic-structure interaction. *Finite Elements in Analysis and Design*, v. 106, p. 56–64, 2015.

52 ZHANG, W. et al. A new topology optimization approach based on moving morphable components (mmc) and the ersatz material model. *Structural and Multidisciplinary Optimization*, v. 53, p. 1243–1260, 2016.

53 WU, C.-Y.; TSENG, K.-Y. Topology optimization of structures using modified binary differential evolution. *Structural and Multidisciplinary Optimization*, v. 42, p. 939–953, 12 2010.

54 SIGMUND, O. On the usefulness of non-gradient approaches in topology optimization. *Structural and Multidisciplinary Optimization*, Springer, v. 43, n. 5, p. 589–596, 2011.

55 GUIRGUIS, D. et al. Evolutionary black-box topology optimization: challenges and promises. *IEEE Transactions on Evolutionary Computation*, IEEE, v. 24, n. 4, p. 613–633, 2019.

56 SEITZ, K. F.; GRABE, J. Three-dimensional topology optimization for geotechnical foundations in granular soil. *Computers and Geotechnics*, v. 80, p. 41–48, 2016.

57 TIAN, X. et al. Topology optimization design for offshore platform jacket structure. *Applied Ocean Research*, Elsevier, v. 84, p. 38–50, 2019.

58 TAVARES, E.; LABAKI, J. Topology optimization of surface structures supported by pile groups. In: *CILAMCE 2019 Proceedings of the XL Ibero-Latin-American Congress on Computational Methods in Engineering, ABMEC*. Natal/RN, Brazil: [s.n.], 2019.

59 SIQUEIRA, A.; PICELLI, R.; LABAKI, J. Topology optimization of tunnel reinforcements using an IBEM-FEM coupling model. *CONEM 2010 XI Congresso Nacional de Engenharia Mec ,nica*, Elsevier, 2022.

60 ALIABADI, M. H. *The boundary element method, volume 2: applications in solids and structures*. [S.l.]: John Wiley & Sons, 2002. v. 2.

61 SOMMERFELD, A. *Partial differential equations in physics*. [S.l.]: Academic press, 1949. v. 1.

62 CHRISTENSEN, R. M. *Theory of Viscoelasticity: Second Edition (Dover Civil and Mechanical Engineering)*. [S.l.]: Dover Publications, 2010. ISBN 048642880X.

63 PIESSENS, R. et al. *Quadpack: A Subroutine Package for Automatic Integration*. [S.l.]: Springer-Verlag, 1983. (Springer Series in Computational Mathematics).

64 WYNN, P. A note on salzer's method for summing certain slowly convergent series. *Journal of Mathematics and Physics*, v. 35, n. 1-4, p. 318–320, 1956.

65 NOCEDAL, J.; WRIGHT, S. J. *Numerical Optimization*. 2nd. ed. Berlin, New York: Springer-Verlag, 2006.

66 HAFTKA, R. T.; GÜRDAL, Z. *Elements of structural optimization*. [S.l.]: Springer Science & Business Media, 2012. v. 11.

67 SIGMUND, O.; PETERSON, J. Numerical instabilities in topology optimization: A survey on procedures dealing with checkerboards, mesh-dependencies and local minima. *Structural Optimization*, v. 16, p. 68–75, 1998.

68 LI, Q.; STEVEN, G. P.; XIE, Y. M. Thermoelastic topology optimization for problems with varying temperature fields. *Journal of Thermal Stresses*, v. 24, n. 4, p. 347–366, 2001.

69 MUNK, D. J.; VIO, G. A.; STEVEN, G. P. Topology and shape optimization methods using evolutionary algorithms: a review. *Structural and Multidisciplinary Optimization*, Springer, v. 52, n. 3, p. 613–631, 2015.

70 LAND, A. H.; DOIG, A. G. An automatic method of solving discrete programming problems. *Econometrica*, v. 28, p. 497–520, 1960.

71 VANDERBEI, R. J. *Linear Programming: Foundations and Extensions*. 4^{th}. ed. [S.l.]: Springer US, 2014.

72 SIGMUND, O. Morphology-based black and white filters for topology optimization. *Structural and Multidisciplinary Optimization*, v. 33, n. 4-5, p. 401–424, 2007.

73 LIANG, Y.; CHENG, G. Further elaborations on topology optimization via sequential integer programming and canonical relaxation algorithm and 128-line MATLAB code. *Structural and Multidisciplinary Optimization*, v. 61, p. 411–431, 2020.